The bactericidal mechanism of lactoferricin B and its fragment revealed by the single GUV method

静岡大学博士論文

The bactericidal mechanism of lactoferricin B and its fragment revealed by the single GUV method

単一巨大リポソーム法により明らかにされたラクトフェリシンＢとそのフラグメントの殺菌活性のメカニズム

MD. MONIRUZZAMAN

大学院自然科学系教育部

バイオサイエンス専攻

2016 年 12 月

Table of Contents

List of abbreviations

AMP	:	antimicrobial peptides
BSA	:	bovine serum albumin
CLSM	:	confocal laser scanning microscopy
CPPs	:	cell penetrating peptides
DIC	:	differential interference contrast
DLS	:	dynamic light scattering
DOPC	:	dioleoylphosphatidylcholine
DOPG	:	dioleoylphosphatidylglycerol
GUV	:	giant unilamellar vesicle
LF	:	lactoferrin
LUV	:	large uniamellar vesicle
LfcinB	:	lactoferricinB
LfcinB(4-9)	:	lactoferrincinB (4-9)
MLV	:	multilamellar vesicle
NMR	:	nuclear magnetic resonance
RH	:	rhodamine
SUV	:	small unilamellar vesicle

CHAPTER 1

1. Introduction

1.1 Antimicrobial peptides (AMPs)

AMPs are peptides that have an ability to kill bacteria, viruses and fungi. They play an important role as a part of the innate immune response. So far more than 500 AMPs have been found (Zhao et al., 2013). Both prokaryotes (e.g., bacteria) and eukaryotes (e.g., protozoan, fungi, plants, insects, and animals) can produce AMPs (Colon et al., 2010). In the organism, tissues and organs are the main source of AMPs and they are considered to be the primary boundary of the innate immune response (Leippe et al., 2002) against viruses, bacteria, and fungi (Colon et al., 2010). In the human body epithelial cells, lymph, phagocytes and gastrointestinal cells are main source of AMPs production (Ganz et al., 2003; Niyonsaba et al., 2002). The important characteristics of AMPs is that they are highly positively charged peptides. Hence, they can bind preferentially with the external surfaces of bacterial membranes which are negatively charged, but cannot bind strongly with the external surface of eukaryote plasma membranes. The secondary structure of most of the AMPs are α-helix and β-sheet. Magainin 2, PGLa, cecropin A and LL-37 form mostly α-helix structure. In contrast, β-defensin and protegrin-1 form β-sheet structure. According to Wang et al. (2004), among 525 peptides, 77 peptides are categorized as α-helix structure, 174 peptides are categorized as β-sheet structure, and the structure of 208 peptides are unknown.

1.2 Lactoferrin (LF) and Lactoferricin B (Lfcin B)

Lfcin B is one of AMPs, which is produced by the hydrolysis of 80 kDa iron-binding glycoprotein, LF. LF is found in fluids of the eyes, nose, respiratory tract, intestine, and elsewhere, and main source is cow and human milk (Coscia et al., 2012, Masson et al., 1966; Baker, 1994; Levay and Viljoen, 1995; Lonnerdal and Iyer, 1995; Kikuchi et al., 2003; Baker and Baker, 2005). LF has been used as a medicine for example, treatment of abdominal abscess, dysentery, and hepatitis C (Ward et al., 2005). Functionally, Lf can bind with Fe^{3+} and transfer them (Metz-Boutique et al., 1984) and as a result, LF controls the consumption of Fe^{3+} in the viscera and transfer the Fe^{3+} in to the cells. (Farnaud and Evans, 2003). Therefore, LF belongs to a transferrin family.

LF in milk is hydrolyzed to various peptides by pepsin under acidic conditions (e.g., in mammal stomach). Lactoferricin (Lfcin) is one of these peptides and it contains N-terminus of LF. Depending on the species of origin, Lfcin from bovine lactoferrin and from human lactoferrin are designated Lfcin B and Lfcin H, respectively. LfcinB has antimicrobial activity. To determine the antimicrobial activity of peptides, minimum inhibitory concentration (MIC) values were used. MIC is the minimum concentration of peptides that can inhibit the bacterial growth. The MIC of Lfcin B and Lfcin H are 6 and 100 µg/ml, respectively (Bellamy et al., 1992; Ghosh et al., 1999). LfcinB is composed of 25 amino acids, with an amino acid sequence of FKCRRWQWRMKKLGAPSITCVRRAF. Thus, LfcinB is a highly positively charged peptide, containing five Arg residues and three Lys residues (Yamauchi et al., 1993). Lfcin B has also a disulfide bond between C3 and C20, although this bond is not important for bactericidal activity (Yamauchi et al., 1993). Lfcin B forms a distorted antiparallel β-sheet in aqueous solution. 3D structure of LfcinB has an amphipathic characters, because it contains a hydrophobic surface (composed of residues F1, C3,
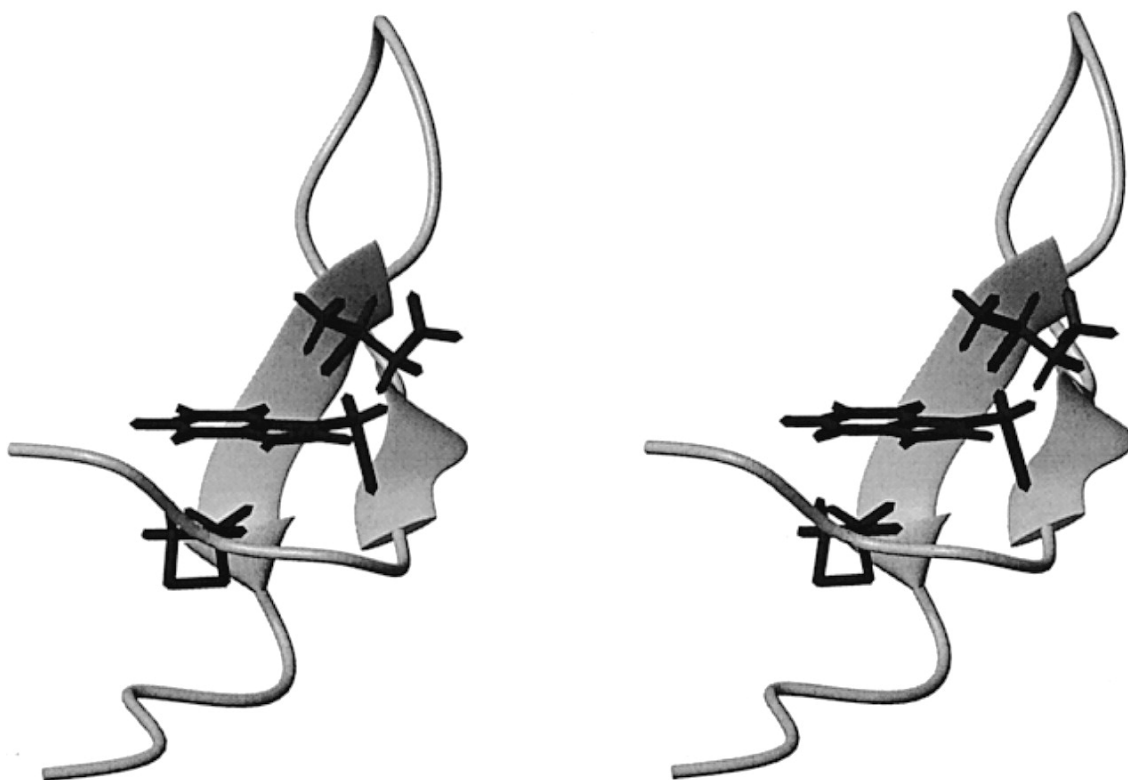
Figure 1.1   Stereo view of a Richardson diagram of LfcinB. (Hwang et al., 1998)

W6, W8, P16, I18, and C20) and a hydrophilic surface comprising of the charged residues at opposite sides (Hwang et al., 1998). This amphipathic structure is similar to that of other AMPs (Zasloff, 2002; Melo, 2009; Hawnget al., 1998). Notably, although Lfcin H with a length of 47 amino acid residues is almost double the size of Lfcin B, it also exhibits an amphipathic structure based on its structural analysis (Hunter et al., 2005). The antimicrobial activity of Lfcin B is much higher than that of Lfcin H (Bellamy et al., 1992) and therefore the majority of research on Lfcins has employed the bovine homolog.

1.3 Derivatives of Lfcin B

Shorter fragment of LfcinB also have an antimicrobial activity (Table 1.1). LfcinB (4-9) has an antimicrobial activity that can be compared with LfcinB (Tomita et al., 1994; Kang et al., 1996; Rekdal et al., 1999; Wakabayashi et al., 1999; Strom et al., 2000 Schibli et al., 2002; Strom et al., 2002; Wakabayashi et al., 2003; Nguyen et al., 2005; Jing et al., 2006). Interaction of LfcinB (4-9) with lipid membranes was investigated based on characteristics of Trp fluorescence and its quenching using fluorescence spectroscopy, indicating that Trp side chain of this peptide locates at near membrane interface (Schibili et al., 2002). The structure of LfcinB (4-14) in sodium dodecyl sulfate (SDS) micelles indicates that it does not form an α-helix but it has an amphipathic characters (Nguyen et al., 2005), which is similar to LfcinB (Hwang et al., 1998). A 15-residue linear fragment of LfcinB (i.e., LfcinB (17-31)) has also a strong antimicrobial activity (i.e., the MIC value of LfcinB (17-31) against *E. coli* was 24 μg), although mutants of LfcinB (17-31) whose Trp6 or Trp8 was replaced with Ala did not have an antimicrobial activity (Rekdal et al., 1999).

4

Table 1.1: Bactericidal activity of LfcinB and their derivatives

Peptide	Structure	MIC (μg/ml)	References
LfcinB	FKCRRWQWRMKKLGAPSITCVRRAF	6	*Bellamy et al., 1992; Ghosh et el., 2002)*
LfcinB (4-9)	RRWQWR-NH$_2$	6	*Tomita et al., 1994*
LfcinB (4-14)	RRWQWRMKKLG	50	*Nguyen et al., 2005*
LfcinB (17-31)	FKCRRWQWRMKKLGA	40	*Rekdal et al., 1999)*

1.4 Interaction of AMPs with lipid membranes

Mechanisms of bactericidal activity of AMPs depend on peptide structures and functions. Currently, the target of AMPs can be categorized into two types; plasma membrane of bacteria and DNA or other proteins in the cytoplasm. In the former case, AMPs damage plasma membrane of bacteria to increase its permeability, and in the other case, AMPs can translocate across the plasma membrane and enter the cytoplasm of bacteria to bind with DNA or other proteins in the cytoplasm. To clarify the mechanism of the AMP-induced damage of plasma membrane of bacteria, interactions of AMPs with lipid membranes have been investigated. For this purpose, a suspension of large unilamellar vesicles (LUVs) of lipid membrane with a diameter of 100-500 nm have been used. For example, the interaction of magainin 2, one of AMPs, with LUVs (Matsuzaki, et. al. 1995; Matsuzaki et. al., 1998; Boggs, et. al., 2001; Gregory, et. al., 2009) exhibited leakage of internal content from vesicles due to the membrane permeation based on the experiment using fluoresce spectroscopy. Investigation on

interaction of Lfcin B with the lipid membrane using the LUV suspension method has revealed that lactoferricin induces leakage of K^+ and H^+ (Aguilera, et al., 1999; Umeyama, et al., 2006; Jing et al., 2006). In these studies, the average values of the physical parameters of vesicles have been obtained from a large number of vesicles, and thereby much information has been lost. There are many causes for the leakage and it is difficult to identify its cause based on the results of the LUV suspension method (Yamazaki, 2008). Although the elementary processes of pore formation are not clear because only the average physical properties of all the LUVs which remain at different elementary processes are obtained using LUV suspension method (Yamazaki, 2008). For example, the interactions of peptides/proteins with lipid membranes, various kinds of changes of physical properties such as size, shape and fluorescence intensity, and also various events such as membrane fusion and vesicle fission has been occurred. Usually these kind of events do not occur simultaneously in all the vesicles, and therefore, an ensemble average of different kinds of stages of these events has been measured.

Based on the data obtained using the LUV suspension method, several models of the AMP-induced damage of lipid membranes for its bactericidal activity have been proposed; In the toroidal pore model, the outer and inner monolayer of membranes bend and merge in a toroidal structure to create a pore in which the inner wall is composed of α-helical peptides and lipid head groups (Brogden, 2005; Wu et al., 1999). In contrast, in the barrel-stave pore model, peptides insert vertically into the lipid membranes and then a fixed number of peptides associate strongly to each other to form an α-helical bundle, which creates a narrow pore with a finite size (Zhang et al., 2001; Ehrenstein et al., 1977; Shimazaki et al., 1998). In this model, the hydrophobic peptide portion coordinates with the lipid core portion and the hydrophilic peptide regions form a pore in the interior region. In the case of carpet model, peptides firstly bind with the outer

part of the target membrane and cover it in a carpet-like fashion (Bahar et al., 2013). Membrane permeation occurred when high concentration of peptides bind with lipid core in case of carpet model (Pouny et al., 1992; Bechinger et al., 2005; Bolintineanu et al., 2011). Recently a stretching model has been proposed (Tamba et al., 2010; Karal et al., 2015); the binding of AMPs to the outer monolayer of a vesicle induces an increase in the area of the bilayers, which induces as stretching the inner monolayer, and as a result, pore formation occurs in the bilayers.

To overcome the disadvantage of the LUV suspension method, the single GUV (Giant unilamellar vesicle) method has been developed (Yamazaki, 2008; Islam et al., 2014). In this model, change of the structure and physical properties of a single GUV that are induced by interactions of compounds such as peptides/proteins with the lipid membrane are observed as a function of time and spatial coordinates. The same experiments are repeated many "single GUVs". The statistical analysis of these results provides the rate constants of the elementary processes underlying the structural changes and functions of GUVs. This single GUV method can reveal details of the elementary processes of individual events, and allow calculation of their kinetic constants. Using the single GUV method, the rate constants of pore formation in lipid membranes induced by the antimicrobial peptide magainin 2 and the rate constant of membrane permeation of various fluorescent probes through these pores have been obtained (Tamba & Yamazaki, 2005; Tamba & Yamazaki, 2009; Tamba et al., 2010, Karal et al., 2015a). This method allows to distinguish pore formation step in membranes from the step of fluorescent probe leakage through the pores, which enables an accurate estimation of the rate constants of both the elementary processes (Tamba et al., 2010). The single GUV method can be also used for the investigation of interactions of cell penetrating peptides (CPPs) with lipid membranes (Islam et al., 2014; Sharmin et

al., 2016). Entry of CPPs into a lumen of single GUVs can be detected. Correlation between the entry of CPPs and pore formation, and also kinetics of entry of CPPs (especially, binding constant and unbinding constant of peptides with lipid membranes) have been revealed (Islam et al., 2014; Sharmin et al., 2016).

1.5. Objectives of the thesis

As described in the section 1.4, the elementary processes and the mechanisms of antimicrobial activity of Lfcin B and its fragments have not been clearly revealed, since the data were obtained using LUV suspension method. To elucidate the mechanism of the antimicrobial activity of Lfcin B and its fragment, I investigated the interaction of these peptides with lipid membranes of GUVs using the single GUV method. For the fragment of Lfcin B, Lfcin B (4-9) was selected because it has one of the strongest antimicrobial activity among all the fragments. I also investigated the interaction of these peptides with *E. coli*.

In the first part, chapter 2, to elucidate the mechanism of the antimicrobial activity of Lfcin B, I investigated the interaction of this AMP with *E. coli* and with liposomes composed of negatively charged dioleoylphosphatidylglycerol (DOPG) and electrically neutral dioleoylphosphatidylcholine (DOPC) mixtures. I found that LfcinB induced leakage of internal contents from GUVs and *E.coli.* To elucidate this mechanism I examined the elementary process and the mechanism of the LfcinB-induced leakage. On the basis of these results, I discussed the mechanism of antimicrobial activity of the Lfcin B.

In the second part, chapter 3, to elucidate the mechanism of the antimicrobial activity of Lfcin B (4-9), I investigate the interaction of LfcinB (4-9) with *E. coli* and

GUVs. I found that LfcinB (4-9) entered the GUVs and *E.coli* without leakage of internal contents from GUVs and *E. coli*. On the basis of this results, I discussed the elementary process and mechanism of antimicrobial activity of LfcinB (4-9) and its translocations across the lipid membranes.

CHAPTER 2

LfcinB-Induced Leakage of Internal Contents from GUVs and *E. coli*

2.1. Introduction

In this chapter, to elucidate the mechanism of the antimicrobial activity of Lfcin B, by investigating the interaction of this AMP with *E. coli* and with liposomes composed of negatively-charged DOPG and electrically-neutral DOPC mixtures. First I investigated the interaction of Lfcin B with *E. coli*. The results indicated that Lfcin B induced the influx of a membrane-impermeant fluorescent probe, SYTOX green, from the extracellular space into the cytoplasm; these data suggested that Lfcin B's bactericidal activity reflects damage to the *E. coli* plasma membrane. Second, Lfcin B-induced leakage of calcein from LUVs and GUVs of 50mol%DOPG/50mol%DOPC (hereafter PG/PC (1/1)) was investigated to permit direct assessment of membrane damage by Lfcin B. Third, to elucidate the mechanism of the Lfcin B-induced calcein leakage, I investigated peptide-induced structural changes in single GUVs. Fourth, I investigated the effects of electrostatic interactions on the Lfcin B-induced calcein leakage using DOPG/DOPC membranes with different DOPG concentration, i.e., 20mol%DOPG/80mol%DOPC (hereafter PG/PC (1/4)). Based on these results, the mechanism of the Lfcin B-induced damage to lipid membranes is discussed.

2.2. Materials and Methods

2.2.1. Materials

DOPC and DOPG were purchased from Avanti Polar Lipids Inc. (Alabaster, AL). Calcein was purchased from Dojindo Laboratory (Kumamoto, Japan). SYTOX green and Texas-Red Dextran 70,000 (TRD-70k) were purchased from Invitrogen, Inc.

(Carlsbad, CA). TRD-70K was used without further purification. Bovine serum albumin (BSA) was purchased from Wako Pure Chemical Industry Ltd. (Osaka, Japan).

2.2.2. Peptide synthesis and identification of peptides

Lfcin B was synthesized by the FastMoc method using a 433A peptide synthesizer (PE Applied Biosystems, Foster City, CA). The sequence of Lfcin B (25-mer) is FKCRRWQWRMKKL-GAPSTICVRRAF with an amide-blocked C terminus. The peptide was cleaved from the resin using trifluoroacetic acid, 1, 2-ethanedithiol, and MilliQ water (9.5/0.25/0.25, volume ratio). Analysis and purification of the peptides were done using reversed phase HPLC, which were described previously (Tamba and Yamazaki, 2005, 2009). The main peak of a HPLC chromatogram of the crude peptides was the reduced Lfcin B (with two sulfhydryl groups) with a mass of 3122.70 Da, and to obtain purified peptides I collected the fraction of main peak, and then lyophilized it. The lyophilized powder was used as the purified peptide. Only one peak was observed in a HPLC chromatogram of the purified peptide, which was the oxidized Lfcin B (i.e., with a disulfide bond) with a mass of 3120.70 Da. The values of mass of the peptides correspond to the molecular masses calculated from the amino acid composition. These results indicate that the reduced Lfcin B was easily oxidized by air. The mass of peptides and identification of the reduced and oxidized Lfcin B were measured using the LC-MS analysis as follows.

LC–MS analysis of the sample was performed by a linear ion trap time-of-flight mass spectrometer (LIT–TOF MS), NanoFrontier eLD (Hitachi High-Technologies Corporation) coupled to a nano-flow HPLC, NanoFrontier nLC (Hitachi High-Technologies Corporation). Two μL of the sample was trapped and desalted with a C18 monolith trap column (0.05 mm ID x 150 mm long; Hitachi High-Technologies

Corporation) and then loaded onto a MonoCap C18 Fast-flow column (0.05 mm ID x 150 mm long; GL Sciences, Inc., Tokyo, Japan) and eluted with a linear gradient from 5 to 100% (v/v) solvent B in 110 min at a flow rate of 200 nL/min. Solvent A was 2% acetonitrile and 0.1% formic acid, and solvent B was 98% acetonitrile and 0.1% formic acid. The eluent was ionized with a nano-electrospray ionization source equipped with an uncoated SilicaTip (New Objective, Woburn, MA) and analyzed with a LIT–TOF MS. The mass spectrum was obtained in positive ion mode at scan mass range m/z 200–2000 and analyzed by the NanoFrontier eLD Data Processing software (Hitachi High-Technologies Corporation).

Lfcin B concentrations in buffer were determined by absorbance using the molar extinction coefficient of Trp at 280 nm (i.e., 5500 $M^{-1}cm^{-1}$).

2.2.3. Measurement of minimum inhibitory concentration (MIC)

The MIC of Lfcin B against *E. coli* (JM-109) was measured using the standard method (Ahmed et al 2010; Andrews et al., 2001). Briefly, a suspension of *E. coli* in Nutrient Broth medium was mixed with various concentrations of Lfcin B solution in the individual wells of a 96-well plate. The final density of bacteria in the wells was 10^5 CFU (colony forming unit) /mL, and the final peptide concentration in the wells ranged from 0.12 to 8.0 μM. After incubation at 37 °C for 18-20 h, the absorbance at 600 nm (Abs (600)) was measured using a microplate reader (Infinite M200, TECAN, Grödig, Austria). The MIC was defined as the lowest concentration of peptide at which there was no change in Abs (600).

2.2.4. Lfcin B-induced influx of SYTOX green into *E. coli*

A suspension of *E. coli* (JM-109) in Nutrient Broth medium was centrifuged (350

× g, 10 min) and the pellet was resuspended in buffer A (10 mM PIPES, pH 7.0, 150 mM NaCl, and 1.0 mM EGTA). To measure the membrane damage of *E.coli,* a membrane impermeant florescent probe, SYTOX green were used. SYTOX green can cross only the dead *E.coli* (see Figure 2.1). Aliquots of this *E. coli* suspension were mixed with SYTOX green in DMSO solution, and then mixed with various concentrations of Lfcin B solution, yielding mixtures with final bacterial densities of $\sim 10^6$ CFU/ml, final SYTOX green concentrations of 5.0 μM, final Lfcin B concentrations of $0 - 50$ μM, and final DMSO concentrations of 0.25% (v/v) (for the experiments of Lfcin B concentration dependence shown in Fig. 2.2A). Immediately after the mixing, we started to measure the fluorescence intensity of the mixture. In separate experiments, aliquots of *E. coli* suspensions at various densities were mixed with SYTOX green in DMSO solution, and then mixed with a given concentration of Lfcin B solution, yielding mixtures with final Lfcin B concentrations of 20 μM and final SYTOX green concentrations of 5.0 μM (for the experiments of the dependence of *E. coli* density shown in Fig. 2.2B). The time courses of fluorescence intensities of these suspensions were measured using a Hitachi F7000 spectrofluorometer (Hitachi, Tokyo, Japan). Fluorescence intensities of samples were measured at the excitation wavelength 480 nm, the emission wavelength 550 nm, and the excitation and emission band-pass 1.5 nm. The temperature of the cell was held at 25 °C with a water bath circulator (Cool-Bit circulator, ACE-05AN, KELK (old name: Komatsu), Ltd., Tokyo, Japan). For 100% permeabilization of *E. coli*, 1.5 mL of the same suspension of *E. coli* without Lfcin B was pelleted by centrifugation (350 × g, 10 min) and the pellet was resuspended in 2.0 mL 70% 2-propanol and allowed to stand at room temperature for 2.0 h. This *E. coli* suspension was pelleted by centrifugation (14000 × g, 20 min, 20 °C) and resuspended in 2.0 mL buffer A. The fluorescence intensity of this suspension
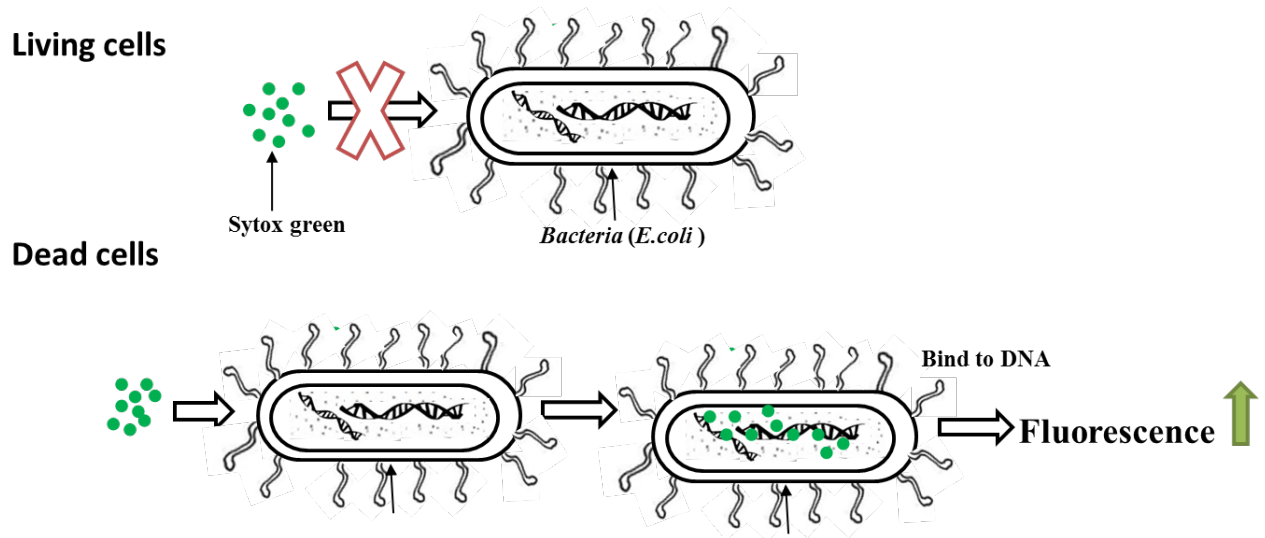
13

Figure 2.1. A schematic diagram of permeabilization of the plasma membrane of *E. coli* by measuring the influx of the membrane-impermeant fluorescent probe, SYTOX green, into the bacterial cytoplasm

under the above conditions was taken as 100% SYTOX influx. The fluorescence intensity of the suspension in the absence of Lfcin B at $t = 0$ was taken as 0% SYTOX influx.

2.2.5. Interaction of Lfcin B with PG/PC (1/1)-LUV suspension

PG/PC (1/1)-LUVs were prepared by the extrusion method (Tamba et al., 2005). First I prepared multilamellar vesicles (MLVs) of PG/PC (1/1) containing calcein solution. For this purpose, 1.0 mL of 70 mM calcein in MilliQ (pH 7.0; adjusted with NaOH) was added to dry lipid film of PG/PC (1/1), and the suspension was vortexed several times for ~20 s at room temperature. Next, the MLV suspension was subjected to five cycles of freezing in liquid N_2 for 1.0 min, followed by warming to room temperature for 25-30 min (freeze-thawing). The resulting solution was extruded through a 200-nm-pore-size Nuclepore membrane using LF-1 LiposoFast apparatus (Avestin, Ottawa, Canada) until the solution became transparent. To remove the untrapped calcein, the LUV suspension was passed through a Sephadex G-75 column equilibrated in buffer A. A Hitachi F7000 spectrofluorometer was used for fluorescence measurement. Fluorescence intensities of samples were measured at the excitation wavelength 490 nm, the emission wavelength 520 nm, and the excitation and emission band-pass 1.5 nm. The temperature of the cell was held at 25°C with a water bath circulator (Cool-Bit circulator). The fluorescence intensity of the PG/PC (1/1)-LUV suspension in the absence of Lfcin B and that in the presence of 0.6% (v/v) Triton X-100 were taken as 0% and 100% leakage, respectively. The lipid concentrations in the sample were determined by the Bartlett method (Bartlett, 1959).

2.2.6. Experiments using the single GUV method

PG/PC-GUVs were prepared by the natural swelling method (Tamba et al., 2005). MilliQ water (20 μL) was added into a dry lipid film in a glass vial (volume: 5 mL), and the mixture was incubated at ~45°C for ~7 min (prehydration), and then incubated with 1.0 mL of buffer A containing 0.10 M sucrose for 2-3 h at 37°C. To obtain a purified GUV suspension, smaller vesicles and untrapped fluorescent probe were removed using the membrane filtering method (Tamba et al., 2011). Briefly, the suspension was centrifuged (14000 × g, 20 min, 20°C); the resulting supernatant was filtered through a Nuclepore membrane with 10-μm diameter pores (Whatman, GE Healthcare, UK, Ltd., Buckinghamshire, UK) in buffer A containing 0.10 M glucose for 1.0 h at a flow rate of 1.0 mL/min at room temperature (20–25°C); the retained suspension (i.e., that which did not pass through the filter) was collected and used as the purified GUV suspension in the following experiments. To prepare GUVs containing water-soluble fluorescent probe, calcein or TRD-70k (i.e., fluorescent probe, texas red (TR)-labeled dextran with average molecular weight of 70k), I used buffer A supplemented with 1.0 mM calcein or with 10 μM TRD-70k for the GUV preparation procedure. After purification, the GUV suspension (~300 μL) was transferred into a hand-made microchamber, which had been formed on a glass slide by inserting a U-shaped silicone-rubber spacer between a cover slip and the glass slide (Yamazaki et al., 2008). To prevent strong interaction between the glass surface and GUVs, the inside of the microchamber was coated with 0.10% (w/v) BSA in buffer A (Zasslof, 2002). The GUVs were observed using an inverted fluorescence phase-contrast microscope (IX-70, Olympus, Tokyo, Japan) maintained at 25 ± 1°C under the control of a stage thermocontrol system (Thermoplate, Tokai Hit, Shizuoka, Japan) (Tamba et al., 2007).

Various concentrations of Lfcin B solution in buffer A containing 0.10 M glucose were continuously added in the vicinity of a GUV through a ~20-μm-diameter glass

micropipette positioned using a micromanipulator. The distance between the GUV and the tip of the micropipette was ~70 μm, and the applied pressure, ΔP (= $P_{in} - P_{out}$, where P_{in} and P_{out} were the pressure of the inside and the outside of a micropipette, respectively) was 30 Pa (Yamazaki et al., 2008). Phase-contrast and fluorescence images of GUVs were recorded using a high-sensitivity EM-CCD camera (C9100-12, Hamamatsu Photonics K.K., Hamamatsu, Japan) with a hard disk. Three ND filters were used to decrease the intensity of the incident light, resulting in conditions where almost no photobleaching of fluorescent probes in a GUV occurred during the interaction of the Lfcin B solution with single GUVs. Thus, under these conditions, the decrease in fluorescence intensity inside a GUV corresponded to leakage of the fluorescent probes from the inside to the outside of the GUV. The fluorescence intensity inside the GUVs was determined using the AquaCosmos software (Hamamatsu Photonics K.K.), and the average intensity per GUV was estimated. The details of this method were described in our previous reports (Yamazaki, 2008).

To obtain the rate constant of the Lfcin B-induced pore formation in lipid membranes (k_P) for various GUVs, the time course of fraction of intact GUV was fit by the exponential decay function using Origin Pro (ver. 8.5, Origin Lab. Corp., Northampton, MA, USA). Three independent experiments were carried out at each Lfcin B concentration to obtain the rate constant, and for each experiment ~20 single GUVs were analyzed to evaluate the rate constant. Mean values and standard errors of the rate constant among the three experiments were calculated.

2.2.7. Measurement of particle size during the interaction of Lfcin B with PG/PC (1/1)-LUV

The size of the LUVs in buffer A was measured at 25 °C using a dynamic light scattering (DLS) apparatus (Zetasizer Nano ZS, Malvern Instrument Ltd., Worcester, UK) (Oka et al., 2014). PG/PC (1/1)-LUVs were prepared by the extrusion method using a 100-nm-pore-size nuclepore membrane (Yamazaki, 2008). Each of the solutions (buffer A, peptide solution, and the LUV suspension) were filtered through a 0.2 μm-pore-size filter (DISMIC-25AS, Advantec Toyo Kaisha Ltd., Tokyo, Japan). The mean particle diameter (Z-average) of the LUVs was obtained by the cumulant method.

2.3. Results and Discussions

2.3.1. MIC of Lfcin B against *E. coli*

First I investigated the antimicrobial activity of the Lfcin B prepared in our laboratory. Using the standard method, we determined the MIC of Lfcin B against *E. coli* (JM-109) as 3 ± 1 μM. This value is consistent with the previously reported value for *E. coli* (0111) (2 μM) (Bellamy et al., 1992).

2.3.2. Lfcin B-induced influx of SYTOX green into cytoplasm of *E. coli*

To clarify the target of Lfcin B's bactericidal activity against *E. coli*, permeabilization of the plasma membrane of *E. coli* was investigated by measuring the influx of the membrane-impermeant fluorescent probe, SYTOX green, into the bacterial cytoplasm. (Roth et al., 1997; Mukherjee et al., 2014). Notably, the fluorescence of SYTOX green is elevated upon binding to nucleic acids; thus increased fluorescence intensity indicates influx of the marker into the cytoplasm. As shown in Figure 2.2A, the fluorescence intensity of SYTOX green increased rapidly with time during the incubation of SYTOX green with an *E. coli* suspension; the increment of the fluorescence intensity also increased with increasing Lfcin B concentration (from 0 to

50 μM). For a given Lfcin B concentration, the increment of the fluorescence intensity rose with decreasing bacterial density; e.g., the SYTOX influx at 600 s increased 4 fold when the bacterial density decreased from 1.0×10^6 to 1.0×10^5 CFU/mL (Figure 2.2B).

Thus, the results of Figure 2.2 indicate that during the interaction of *E. coli* with Lfcin B its plasma membrane was rapidly damaged and as a result SYTOX green permeabilized through the plasma membrane to enter the inside of *E. coli*. This suggests that bactericidality reflects the Lfcin B-induced damage of *E. coli* plasma membrane. Figure 2.2A shows that the fraction of bacteria with damaged plasma membrane increased with an increase in Lfcin B concentration in the buffer outside the bacteria. Figure 2.2B shows that the fraction of bacteria with damaged plasma membrane increased with a decrease in the bacterial density. This can be explained by the decrease in the effective concentration of Lfcin B in the buffer outside the bacteria with an increase in bacterial density because binding of Lfcin B to the membranes of bacteria decreases the Lfcin B concentration in the buffer. A similar phenomena was observed when peptides interact with LUVs in a suspension (see the below section) (Yamazaki, 2008).

2.3.3. Induction of calcein leakage from PG/PC (1/1)-LUVs by Lfcin B

To examine directly membrane damage by Lfcin B and to confirm the target of Lfcin B, I investigated the interaction of Lfcin B with PG/PC (1/1)-LUVs encapsulating a water-soluble fluorescent probe (calcein) using the standard LUV suspension method. Figure 2.3A shows the time course of the leakage (i.e., the efflux) of calcein from the inside of the LUVs following exposure to various concentrations of Lfcin B. The fraction of leakage increased with time over 10 min for 1.0 to 10 μM Lfcin B, and the rate of leakage increased with Lfcin B concentration. At concentrations of ≤0.50 μM
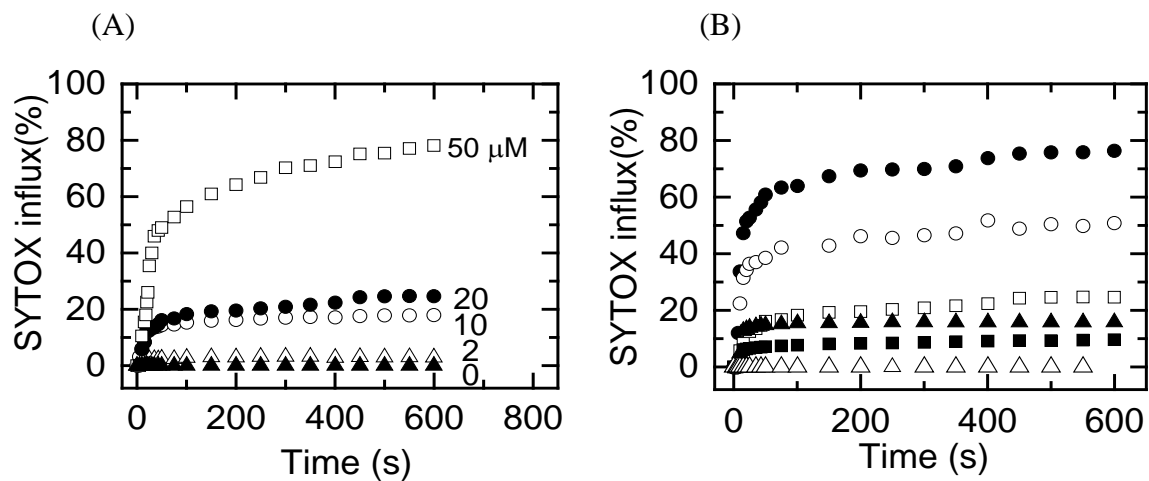
Figure 2.2

Figure 2.2: Time course of influx of SYTOX green into cytoplasm of *E. coli*. (A) Time course of fluorescence intensity of SYTOX green during the interaction of various concentrations of Lfcin B with *E. coli* suspension at 25 °C. Lfcin B concentration is described at the right of each curve. Bacteria density was 1.0×10^6 CFU/mL. (B) Time course of fluorescence intensity of SYTOX green during the interaction of 20 μM Lfcin B with suspensions of various density of *E. coli* at 25 °C. Final bacterial densities were 1.0×10^5 (●), 1.4×10^5 (○), 1.0×10^6 (□), 1.0×10^7 (▲), 1.5×10^7 (■), and 0.0 CFU/mL (△).

Lfcin B, no leakage was observed over 10 min. In contrast, the rate of leakage induced at a higher concentration of Lfcin B (5.0 μM) increased with a decrease in lipid concentration (i.e., LUV concentration) (Figure 2.3B).

These results indicated that Lfcin B induced damage of membrane structure of the LUVs, thereby causing leakage of calcein from the inside of the LUVs. However, there can be many causes for the leakage of water-soluble fluorescent probes; such as pore formation, membrane fusion, large shape changes, and vesicle rupture; it can be difficult to identify the cause of the leakage based on the results of the LUV suspension method. I also noted that the rate of leakage correlated negatively with increase of lipid concentration. This can be explained by the decrease in the effective concentration of Lfcin B in the buffer with an increase in LUV concentration because binding of Lfcin B to the LUV membranes decreases the Lfcin B concentration in the buffer (Yamazaki, 2008).

2.3.4. Induction of calcein leakage from PG/PC (1/1)-GUVs by Lfcin B

To elucidate the process of Lfcin B-induced leakage of calcein from the LUVs, I investigated the interaction of Lfcin B with single PG/PC (1/1)-GUVs containing calcein and 0.10 M sucrose using the single GUV method (Yamazaki, 2008; Islam et al., 2014). The interaction was carried out in buffer A containing 0.10 M glucose at 25 °C. During observation of a single GUV by phase-contrast fluorescence microscope, the tip of a micropipet was approached to the GUV at $t = 0$ and the Lfcin B solution was continuously added from the micropipet into the vicinity of the GUV. Figure 2.4A shows typical experimental results following the interaction of a single GUV with 2.0 μM Lfcin B. Prior to Lfcin B addition, a phase-contrast microscopic image of the GUV indicated a high contrast in the GUV (Figure 2.4A-1) due to the difference in the

Figure 2.3

(A)   (B)
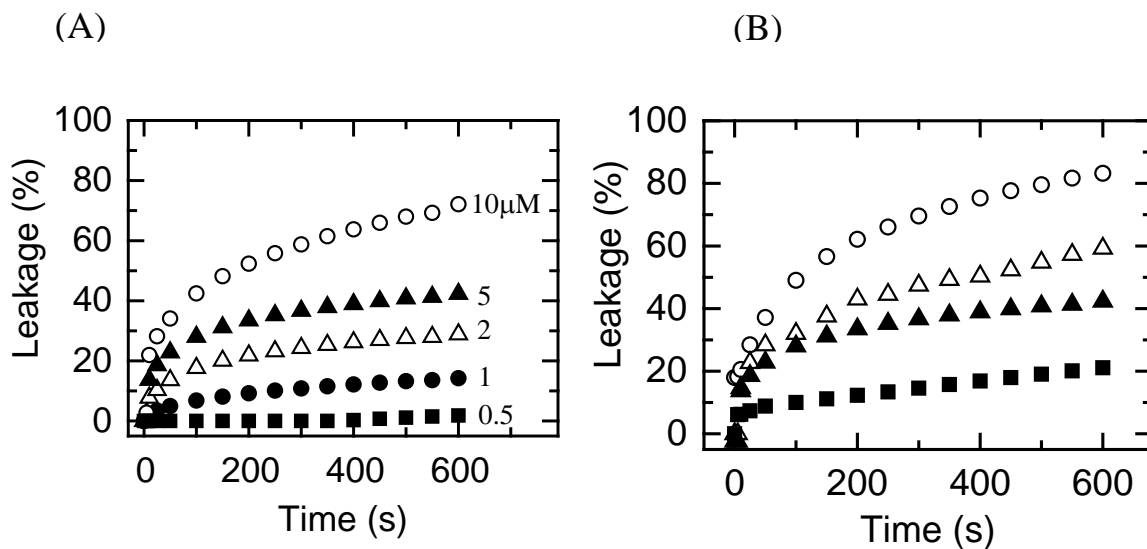
Figure 2.3: Lfcin B-induced leakage of calcein from LUVs. (A) Time course of Lfcin B-induced leakage of calcein from a suspension of PG/PC (1/1)-LUVs after addition of various concentrations of Lfcin B at 25 °C. Final Lfcin B concentration is described at the right of each curve. Lipid concentration was 25 μM. (B) Time course of 5.0 μM Lfcin B-induced leakage of calcein from suspensions of various concentrations of PG/PC (1/1)-LUVs at 25 °C. Lipid concentrations were 1.6 μM (○), 2.5 μM (Δ), 25 μM (▲), and 380 μM (■).

saccharide concentrations between the inside (0.10 M sucrose) and the outside (0.10 M glucose) of the GUV. A fluorescence microscopic image of the same GUV (Figure 2.4A-2) showed a high concentration of calcein inside the GUV at this time. During the addition of the 2.0 μM solution of Lfcin B, the fluorescence intensity inside the GUV was almost constant over the first 143 s, following which the fluorescence intensity decreased suddenly (Figure 2.4A-2, 2.4B). After 146 s the fluorescence intensity fell to effectively zero; a phase-contrast image of the same GUV (Figure 2.4A-3) showed that the spherical GUV structure remained, albeit with an apparent decrease in diameter. As discussed in our previous reports (Tamba and Yamazaki, 2005) the rapid decrease in fluorescence intensity occurred as a result of the leakage of the fluorescent probe through the peptide/protein-induced pores in the lipid membranes. Thus the time at which the fluorescence intensity began to rapidly decrease corresponded to the time at which a pore was formed in the membrane. When the same experiments were carried out using 20 single GUVs, we observed a stochastic occurrence of a similar rapid leakage of calcein from each GUV (Figure 2.4C). The concentration of fluorescent probe inside a GUV is proportional to the fluorescence intensity of the inside of the GUV. In the time course of fluorescence intensity inside the GUV (such as Figure 2.4B and 2.4C), the time when the normalized fluorescence intensity inside the GUV starts to decrease corresponds to the time of pore formation in the lipid membrane. In other words, if the normalized fluorescence intensity inside the GUV is 1.0, no leakage of the fluorescent probe occurs and therefore the state of this GUV corresponds to the intact state. On the other hand, if the normalized fluorescence intensity is less than 1.0, some leakage of the fluorescent probe occurs and therefore the state of this GUV corresponds

Figure 2.4   (A)

(B)

(C)

(D)

(E)
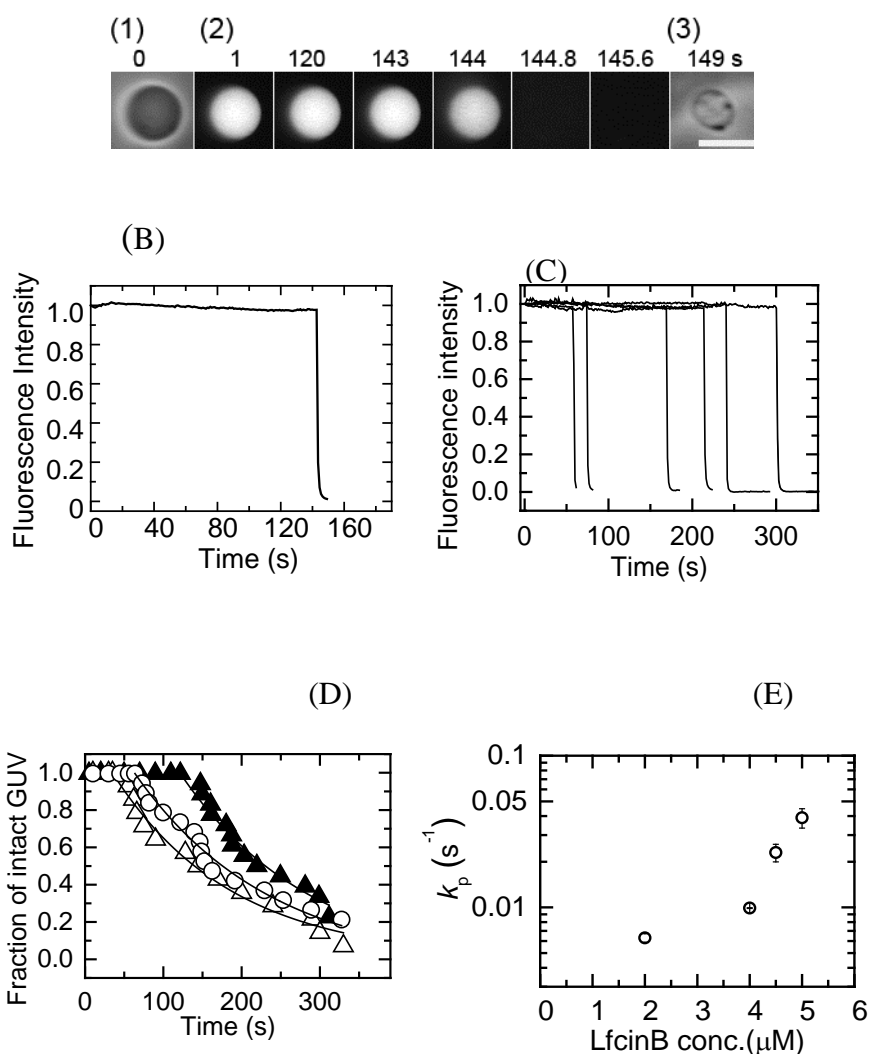
Figure 2.4: Membrane permeation of calcein from single PG/PC (1/1)-GUVs induced by Lfcin B. (A) Leakage of calcein from single PG/PC (1/1)-GUVs was induced by 2.0 μM Lfcin B in buffer A at 25 °C. Fluorescence images (2) show that the calcein concentration inside the GUV rapidly decreased after the addition of Lfcin B. The numbers above each image show the time in seconds after the Lfcin B addition was started. Also shown are phase contrast images of the GUV at time 0 (1) and 149 s (3). The bar corresponds to 20 μm. (B) Time course of the change in the normalized fluorescence intensity of the GUV shown in (A). We defined the normalized fluorescence intensity of the intact GUV before the initiation of the membrane permeation as 1.0. (C) Other examples of the time course of the change in the normalized fluorescence intensity of several "single GUVs" under the same conditions as in (A). (D) Time course of fraction of intact GUV, P_{intact}, of PG/PC (1/1)-GUV. (Δ) shows the data including the results shown in (C). (○) and (▲) show the time course of P_{intact}, of other independent experiments. Solid lines represent the best fit curves of eq. 2.1. (E) Lfcin B concentration dependence of the rate constant of pore formation, k_P. Mean values and standard errors are shown.

24

to the pore state. As we demonstrated in the papers on peptide-induced pore formation,(Islam et.al 2014; Tamba et.al., 2009) the rate constant of Lfcin B-induced pore formation in lipid membranes can be obtained by analyzing the time course of the fraction of intact state of GUVs (i.e., those from which the fluorescent probe did not leak) among the examined GUVs, $P_{intact}(t)$, over time t. Figure 2.4D (Δ) shows that the value of P_{intact} of PG/PC (1/1)-GUVs decreased with time during the interaction with 2.0 µM Lfcin B. The curve of the time course of P_{intact} (Δ) was well fit by a single exponential decay function defined by eq. 2.1, as follows,

$$P_{intact}(t) = \exp\left\{-k_P(t - t_{eq})\right\} \tag{2.1}$$

where k_P is the rate constant of the Lfcin B-induced pore formation and t_{eq} is a fitting parameter which denotes the time required for the binding equilibrium of LfcinB from aqueous solution to the GUV membrane (Islam et al., 2014;   Tamba et al., 2007). To determine the mean value for k_P, three independent experiments ($n = 3$) using 20 single GUVs to obtain the time course of P_{intact} were carried out and these curves were also well fit by eq. 2.1 (Figure 2.3D). The mean value of k_P for 2.0 µM Lfcin B was $(6.3 \pm 0.5) \times 10^{-3}$ s^{-1} ($n = 3$). The values of the fitting parameter t_{eq} have larger variation compared with those of k_P. The value of t_{eq} includes the time required for attaining equilibrium concentration of LfcinB in the vicinity of a GUV because we started to add the LfcinB solution from the tip of the micropipet to the vicinity of a GUV at $t = 0$. Therefore the value of t_{eq} depends on the size and the shape of the micropipet tip and the setting of micropipet inside a microchamber, which have some variation in each experiment. This is one of the main reasons of the larger variation of t_{eq}.

I also investigated the effect of Lfcin B concentration on the rate constant of pore formation. At concentrations of ≥1.0 μM Lfcin B, leakage of calcein like that shown in Figure 2.4C was observed. This assay was used to determine the rate constant of pore formation (k_P) at concentrations of ≥2.0 μM Lfcin B (Figure 2.4E). k_P increased with Lfcin B concentration. At 4.5 and 5.0 μM k_P values were greater than 2×10^{-2} s^{-1}.

2.3.5. Lfcin B-induced structural change in single PG/PC (1/1)-GUVs

To elucidate the decrease in diameter of the GUVs after its interaction of LfcinB, we investigated the process of the structural change of single GUVs using the phase contrast microscopy. Figures 2.5A shows a typical example of 5.0 μM Lfcin B-induced transformation of a PG/PC (1/1)-GUV. As shown in phase-contrast microscopic images in Figure 2.5A, at 21.13 s the sucrose solution inside the GUV suddenly started to diffuse to the outside of the GUV. From 21.13 to 21.16 s, the diameter of the GUV rapidly decreased; from 21.16 s, the diffusional flow of sucrose solution could not be observed. At 21.16 s the phase contrast of the inside of the GUV became small: although the spherical shape of the GUV was still visible, a large area of thicker membrane region with higher contrast and several small high-contrast (black) particles appeared on the membrane of the GUV. Figure 2.5B shows a typical example of the 2.0 μM Lfcin B-induced transformation of a PG/PC (1/1)-GUV. Similar structural changes were observed in this GUV, including the rapid leakage of sucrose, but the leakage process started at 77.59 s and completed at 77.65 s within 66 ms. The results of Figure 2.5 clearly indicate that LfcinB induced a transient, rapid leakage of sucrose from the single GUVs and then smaller spherical GUVs remained. It is inferred that part of the GUV membrane was lost, and postulate that the large areas of the thicker, increased-contrast membrane and small high-contrast (black) particles on the membrane

Figure 2.5

(A)

(B)

(C)

(D)
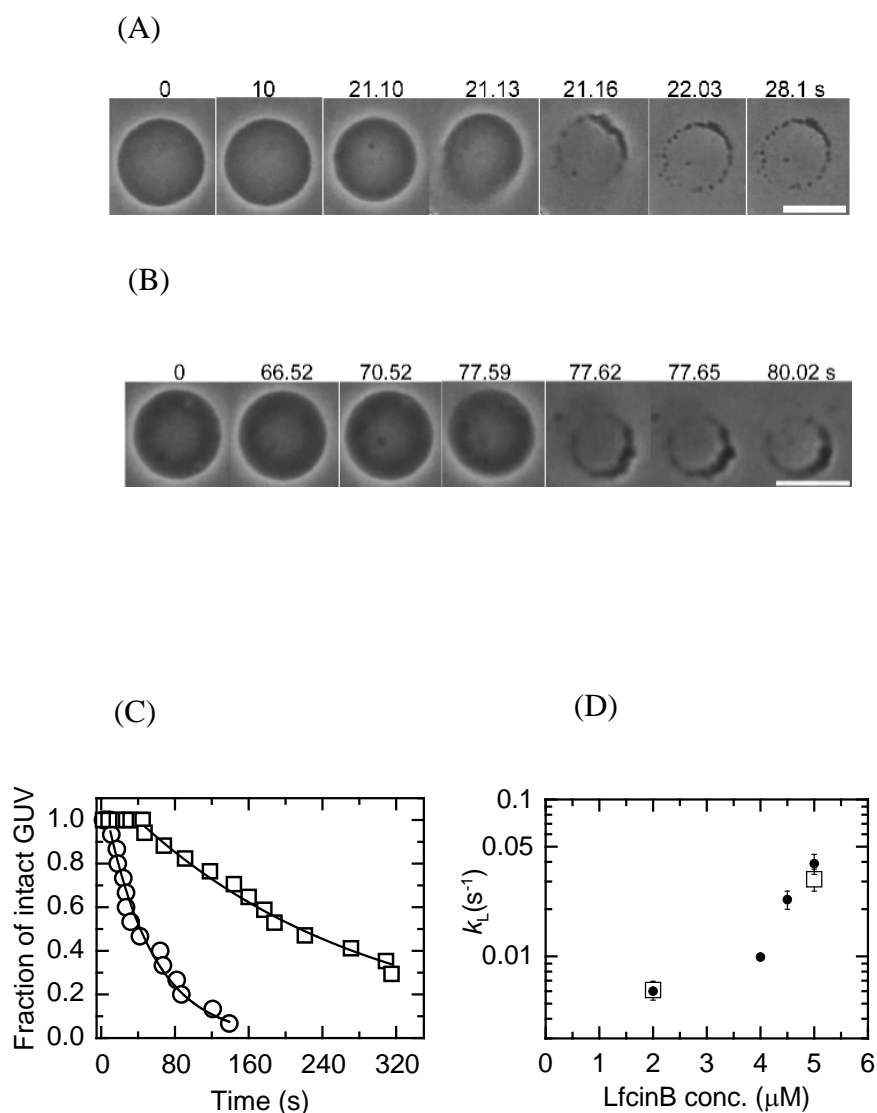
Figure 2.5: Structural change of single PG/PC (1/1)-GUVs induced by Lfcin B. Phase contrast images of single GUVs in the interaction of (A) 5.0 μM and (B) 2.0 μM Lfcin B in buffer A at 25 °C. The numbers above each image show the time in seconds after the Lfcin B addition was started. The bar corresponds to 20 μm. (C) Rate constant of Lfcin B-induced local rupture of PG/PC (1/1)-GUVs. Time course of the fraction of intact GUVs which was identified by its phase-contrast microscopic image, $P_{intact}(t)$, in the presence of 2.0 μM (□) and 5.0 μM (○) Lfcin B. (D) The Lfcin B concentration dependence of the rate constant of local rupture, k_L (□). For comparison, the Lfcin B concentration dependence of the rate constant of pore formation, k_P, (the same as Figure 2.4E) was also plotted (●).

27

correspond to a complex of lipid membranes and Lfcin B (see the details in the Discussion section). Due to the very fast leakage, and at the present time resolution of the experiments (33 ms), the evolution of pore as would not followed in other similar studies (Tamba et al., 2007). Several words have been used to explain such a rapid leakage of sucrose; large pore formation, local rupture, burst of membranes, and rupture of membranes. Due to the limited time-resolution (i.e., 33 ms) in experimental system, the structural changes of the GUV during the rapid leakage of sucrose were not reveal completely. Therefore at present stage it cannot identify the elementary processes and the mechanism of the rapid leakage. Here I use the word of "local rupture" tentatively to express the rapid leakage of sucrose and the survival of spherical structure of GUVs. Previously, this word (local rupture) was used for the similar phenomena induced by a peptide, transportan 10 (Islam et al., 2014).

The above results suggested that the leakage of calcein from inside single GUVs occurred as a result of local rupture in the GUV membranes. To confirm the correlation between the leakage of calcein and local rupture in GUVs, the rate constant of local rupture was calculated. For this calculation, it is considered the conversion from the intact state of GUV to the ruptured state of GUV in which sucrose has been already leaked or is leaking as a two-state transition. The concentration of sucrose inside a GUV is proportional to the phase contrast of the inside of the GUV. In the consecutive phase contrast images (such as Figure 2.5A and 2.5B) at the time resolution of 33 ms, the time of the image in which the rapid leakage of sucrose started from a GUV (e.g., 21.13 s in Figure 2.5A and 77.59 s in Figure 2.5B) corresponds to the time of local rupture. Therefore the state of the GUV before the time of local rupture corresponds to the intact state, and the state of the GUV at and after this time corresponds to the ruptured state. The rate constant of the two-state transition from the intact state to the rupture state (i.e.,

the rate constant of local rupture), k_L, can be determined from the fraction of intact state of GUVs (i.e., the fraction of intact GUVs), designated as $P_{intact}(t)$. Figure 2.5C shows the time course of $P_{intact}(t)$ in the presence of 2.0 µM Lfcin B. The fraction of the intact GUV can be expressed using the rate constant, k_L, as follows:

$$P_{intact}(t) = \exp\{-k_L(t - t_{eq})\}$$ (2.2)

where t_{eq} is an adjustable parameter. This equation is almost the same as that for the rate constant of the EGCg-induced burst of a GUV (Tamba et al., 2007). All the curves of the time course of the $P_{intact}(t)$ were well fit by eq. 2.2 (Figure 2.5C). The rate constant k_L increased with increasing Lfcin B concentration: at 2.0 and 5.0 µM Lfcin B, the k_L values were $(7.0 \pm 0.2) \times 10^{-3}$ s^{-1} and $(3.6 \pm 0.2) \times 10^{-2}$ s^{-1}, respectively ($n = 3$ for each concentration). These results indicated that the Lfcin B-induced local rupture in the GUV membrane apparently followed the first-order reaction. The values of k_L and k_P against Lfcin B concentrations were the same within an experimental error (Figure 2.5D). These results clearly indicate that the leakage of calcein from the inside to the outside of single GUVs occurred as a result of local rupture in the GUV membrane and that the smaller sizes of pores were not formed before the local rupture. This result supports the above hypothesis on the two-state transition for the formation of the local rupture.

2.3.6. Induction of TRD-70k leakage from PG/PC (1/1)-GUVs by Lfcin B

In order to examine the size of the Lfcin B-induced pores in lipid membranes, I investigated the leakage of a water-soluble fluorescent probe, TRD-70k, using the single GUV method. The molecular weight distribution of TRD-70k is 60,000–90,000

Figure 2.6

(A)

(1) (2) (3)
0 1 50 76.20 77.33 78.51 82.88 85 s

(A)

(D)
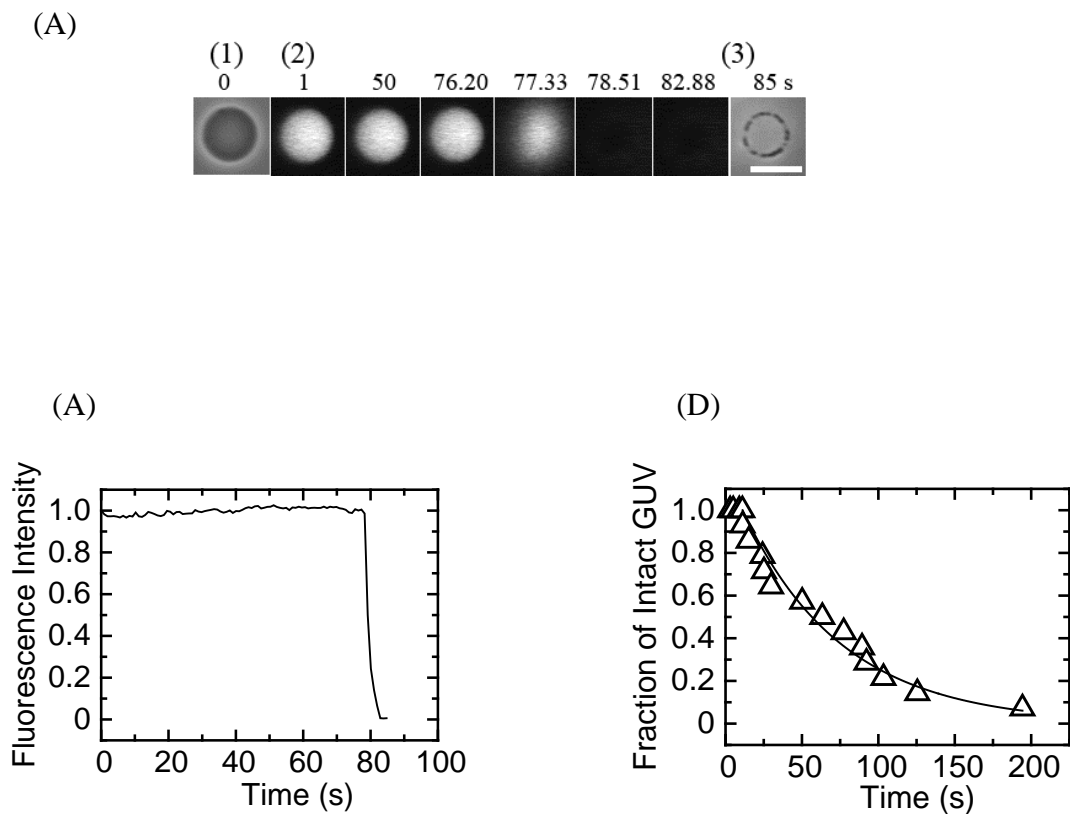
Figure 2.6: Membrane permeation of TRD-70k from single PG/PC (1/1)-GUVs induced by Lfcin B. (A) Leakage of TRD-70k from single PG/PC (1/1)-GUVs induced by 5.0 μM Lfcin B in buffer A at 25 °C. (A) Fluorescence images (2) show that the TRD-70k concentration inside the GUV rapidly decreased during the addition of Lfcin B. The numbers above each image show the time in seconds after Lfcin B addition was started. Also shown are phase contrast images of the GUV at time 0 (1) and 85 s (3). The bar corresponds to 20 μm. (B) Time course of the change in the normalized fluorescence intensity of the GUV shown in (A). (C) Time course of P_{intact} of PG/PC (1/1)-GUV containing TRD-70k in the presence of 5.0 μM Lfcin B in buffer A at 25 °C. The solid line represents the best fit curve using eq. 2.1

according to the manufacturer, and its Stokes-Einstein radius, R_{SE}, is 6.4 nm (Goins A.B., 2008). Figure 2.6A shows the effect of 5.0 μM Lfcin B on single PG/PC (1/1)-GUVs pre-loaded with TRD-70k. Prior to Lfcin B addition, a phase-contrast microscope image of the GUV showed high contrast (Figure 2.6A-1) due to the difference in the saccharide concentration between the inside (0.1 M sucrose) and the outside (0.1 M glucose) of the GUV. A fluorescence microscope image of the same GUV (Figure 2.6A-2) showed a high concentration of TRD-70k inside the GUV at this time. During addition of a 5.0 μM solution of Lfcin B, the fluorescence intensity inside the GUV remained similar over the first 77.30 s, but at 77.33 s a rapid decrease in the fluorescence intensity was observed (Figure 2.6A-2, B). After 82.89 s, the fluorescence intensity approached zero, although a phase-contrast image of the same GUV (Figure 2.6A-3) showed that the GUV retained its spherical structure, albeit with a decreased diameter. These data indicate that TRD-70k passed through Lfcin B-induced pores in the GUV membrane. When the same experiments were carried out using 20 single GUVs, similar leakage of TRD-70k from a GUV was observed to occur in a stochastic fashion. Figure 2.6C shows that the curve of the time course of P_{intact} was well fit by eq. 2.1. The average value of k_P for 5.0 μM Lfcin B was $(2.1 \pm 0.4) \times 10^{-2}$ s^{-1} ($n = 3$). This k_P value is smaller than that obtained using PG/PC (1/1)-GUVs containing calcein. Based on the results of Figure 2.5 and 2.6, it is inferred that the radius of the Lfcin B-induced pore is greater than 6.4 nm (i.e., R_{SE} of TRD-70k).

2.3.7. Effects of electrostatic interactions on Lfcin B-induced pore formation in single PG/PC-GUVs

It has been reported that the binding constant of Lfcin B with lipid membranes increases with an increase in contents of negatively charged lipids such as phosphatidylglycerol,

suggesting that the electrostatic interactions between Lfcin B and the lipid membrane play an important role in the binding of Lfcin B. To control electrostatic interactions of lipid membranes in water, it can be change surface charged density of the membranes or salt concentrations (Israelachvili, 1992; Mclaughlin et al., 2005; Karal et al., 2015). The surface charge density can be controlled by the concentration of negatively-charged lipid (i.e., PG) in the PG/PC membranes. First, to elucidate the effects of the surface charge density on the Lfcin B-induced pore formation, it was investigated the interaction of Lfcin B with single PG/PC (1/4)-GUVs containing calcein. Lfcin B at concentrations of ≤5.0 μM did not induce calcein leakage. However, at concentrations of ≥10 μM Lfcin B, leakage of calcein similar to that seen in Figures 2.4A and C was observed. Figure 2.7A shows the time course of P_{intact} of PG/PC (1/4)-GUVs interacting with various concentrations of Lfcin B; these data were well fit by eq. 2.1. For example, the mean value of k_P for 20 μM Lfcin B was $(5.4 \pm 0.3) \times 10^{-3}$ s^{-1} ($n = 3$). As shown in Figure 2.7B, at concentrations of ≥15 μM Lfcin B, the rate constant of pore formation k_P was determined and k_P increased with Lfcin B concentration. It is evident that higher concentrations of Lfcin B were required to induce pore formation in PG/PC (1/4)-GUVs than in PG/PC (1/1)-GUVs. This result suggests that the activity of Lfcin B-induced pore formation increases with the surface charge density of the membrane. As an alternative explanation, the PG concentration, rather than the surface charge density, may play a role in Lfcin B-induced pore formation.

Next, to elucidate the effects of the salt concentration on the Lfcin B-induced pore formation, we investigated the interaction of Lfcin B with single PG/PC (1/1)-GUVs in buffer A without NaCl (10 mM PIPES, pH 7.0, 1.0 mM EGTA). At concentrations of

Figure 2.7

(A)

(B)

(C)

(D)
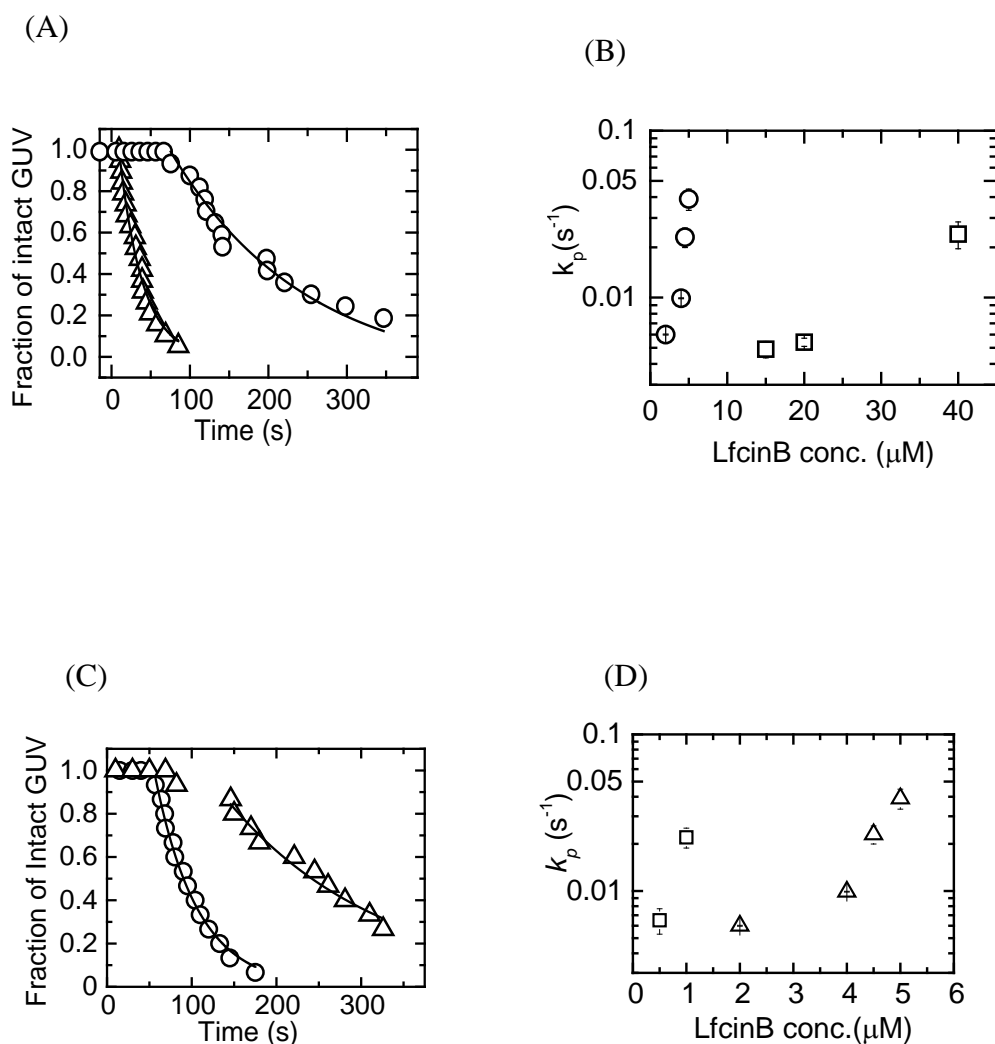
Figure 2.7: Effects of electrostatic interactions on Lfcin B-induced pore formation. (A) Time course of P_{intact} of PG/PC (1/4)-GUV containing calcein in buffer A during the interaction of various concentrations of Lfcin B. (Δ) 40 μM, and (○) 20 μM Lfcin B. Solid lines represent the best fit curves of eq 2.1. (B) The Lfcin B concentration dependence of the rate constant of pore formation, k_P in PG/PC (1/4)-GUV (□). For comparison, the same data for PG/PC (1/1)-GUV was also plotted (○) (this is the same data as in Figure 2.8E). Mean values and standard errors were shown. (C) Time course of P_{intact} of PG/PC (1/1)-GUV containing calcein in buffer A without NaCl (10 mM PIPES, pH 7.0, 1.0 mM EGTA) during the interaction of various concentrations of Lfcin B. (○) 1.0 μM, and (Δ) 0.5 μM Lfcin B. A solid line represents the best fit curve of eq 2.1. (D) The Lfcin B concentration dependence of the rate constant of pore formation, k_P in PG/PC (1/1)-GUV in buffer A without NaCl (10 mM PIPES, pH 7.0, 1.0 mM EGTA) (□). For comparison, the same data for PG/PC (1/1)-GUV was also plotted (Δ) (this is the same data as in Figure 2.8E). Mean values and standard errors were shown

≥1.0 µM Lfcin B, leakage of calcein similar to that seen in Figures 2.4A and C was observed. Figure 2.7C shows the time course of P_{intact} of PG/PC (1/1)-GUVs interacting with various concentrations of Lfcin B; these data were well fit by eq. 2.1. As shown in Figure 2.7D, the mean value of k_P for 1.0 µM and 0.5 µM Lfcin B were $(2.2 \pm 0.3) \times 10^{-2}$ s^{-1} ($n = 3$) and $(6.5 \pm 1.2) \times 10^{-3}$ s^{-1} ($n = 3$), respectively. It is evident that lower concentrations of LfcinB induced pore formation in buffer A without NaCl than that in buffer A containing 150 mM NaCl (i.e., the k_p values in 0 mM NaCl were greater than those in 150 mM NaCl). Electrostatic interactions in buffer increase with a decrease in salt concentration because shielding of the membrane surface charge by counterions decreases (i.e., the Debye length increases), (Israelachvili, 1992; Mclaughlin et al., 2005; Karal et al., 2015). So Figure 2.7D indicates that k_p increases with an increase in the extent of electrostatic interactions.

Both the results of the effect of the surface charge density and that of salt concentration on k_p clearly show that k_p increases with an increase in the extent of electrostatic interactions due to membrane surface charges. One of main factors of the binding of Lfcin B with PG/PC membranes is the electrostatic attraction between the positively-charged peptide and the negatively-charged membranes. This electrostatic interaction increases with an increase in surface charge density (i.e., the increase of the negatively-charged DOPG concentration) or a decrease in salt concentration. Therefore, when Lfcin B concentration in buffer is the same, its surface concentration in the membrane increases with an increase in the electrostatic interaction. It is reported that the surface concentration of magainin 2 determines the rate constant of pore formation for the interaction of positively-charged magainin 2 with negatively-charged PG/PC membranes. Therefore, the results in Figure 2.7 suggest that the surface concentration of Lfcin B is one of key factors for pore formation.

Figure 2.8
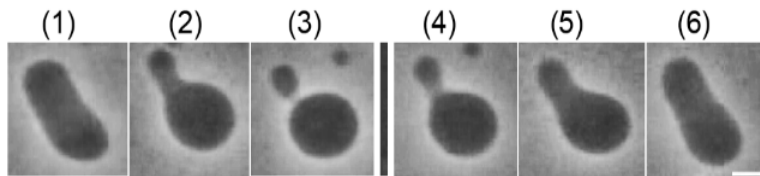
Figure 2.8: Shape change of a PG/PC (1/4)-GUV induced by the interaction of Lfcin B and its reversibility. (1) −(3) after the addition of 0.20 μM Lfcin B, a prolate changed into a pear, and then into a two spheres connected by a narrow neck. The time after the addition of Lfcin B through the micropipet is (1) 0 s, (2) 66 s, and (3) 82 s. (4)−(6) After the addition of Lfcin B was stopped, the shape change was reversed. The time after stopping the addition of Lfcin B is (4) 125 s, (5) 151 s, and (6) 208 s. The bar corresponds to 20 μm.

2.3.8. Lfcin B-induced shape changes in single PG/PC (1/4)-GUVs

To elucidate how Lfcin B interacts with the PG/PC membranes, I investigated its effect on the shapes of PG/PC (1/4)-GUVs upon addition of Lfcin B. It is well known that analysis of substance-induced shape changes of GUVs is a highly sensitive method for detecting the interaction of substances with lipid membranes (Farge et al., 1992; Tanaka et al., 2002; Yamashita et al., 2002). Generally, there are various shapes of GUVs such as sphere, prolate, cylinder, and discocyte. The shapes of GUVs are determined based on some parameters such as area difference between outer and inner monolayers and the volume to the area ratio of the GUV when they are formed. Generally it was selected GUVs based on their shape depending on the purpose of experiments. In this experiment I selected spherical GUVs for leakage experiments and prolate GUVs for shape change experiments. The probability of formation of prolates in PG/PC (1/1)-GUVs was much lower than that of PG/PC (1/4)-GUVs. Hence here we investigated the effects of the interaction of Lfcin B with membranes on the shape of prolate PG/PC (1/4)-GUVs. In the absence of Lfcin B, a GUV had a prolate shape (Figure 2.8(1)). After starting the addition of 0.20 μM Lfcin B, the GUV changed into a pear-like structure (Figure 2.8 (2)), subsequently changed into the shape of two-spheres-connected by a neck (Figure 2.8 (3)). This shape change was observed in 7 of 8 examined GUVs. In order to determine the reversibility of this shape change, the addition of Lfcin B was stopped after the complete shape change of the GUV, and observation was continued. Figure 2.8 (4) −(6) show the time course of the shape change of the GUV after the addition of Lfcin B was stopped. First, the two-spheres-connected by a neck changed into a pear (Figure 2.12 (5)); the pear then reverted into a prolate shape (Figure 2.8 (6)). It is reasonably considered that after the addition of Lfcin B was stopped, remaining Lfcin B diffused away from the vicinity of the GUV into the bulk

solution, inducing a decrease in the Lfcin B concentration near the GUV; the local concentration of peptide in the membrane presumably then decreased (i.e., Lfcin B molecules in the outer monolayer of the GUV transferred into the aqueous solution). This result indicates that the shape change in PG/PC (1/4)-GUV induced by addition of 0.20 μM Lfcin B was reversible. The threshold concentration of Lfcin B for the shape change from a prolate to two spheres connected by a neck (i.e., the Lfcin B concentration at which the shape change occurred in 50% of examined GUVs) was 0.15 μM. The reversibility of the shape change was observed in all the examined GUVs (n = 7).

The results in Figure 2.8 clearly show that low concentrations of Lfcin B (well below the threshold concentration of pore formation of GUV) induced shape changes in PG/PC (1/4)-GUVs. What is the mechanism for these shape changes? It is well established that the shape of a GUV is determined by the minimization of the elastic energy of the closed membrane and that the "area-difference-elasticity" model (ADE model) reasonably explains shape changes of GUVs (Heinrich et al., 1993, Miao et al, 1994). In the ADE model, the area of each monolayer is not fixed to the equilibrium area, but the monolayer membrane can stretch elastically to increase the membrane's nonlocal elastic energy. Thus, the elastic energy of the GUV (W_{el}) can be expressed as a sum of the membrane bending energy and the energy of the relative monolayer stretching. In the ADE model, the shape of the GUV is determined by the minimization of the membrane elastic energy (W_{el}) for a given area A, volume V, and the difference ($\Delta A_0 (= A_0^{out} - A_0^{in})$) between the area of the outer (A_0^{out}) and the inner monolayers (A_0^{in}) in the GUV bilayer membrane under the relaxed (i.e., nonstretched) condition (Heinrich et al., 1993; Miao et al., 1994). An analysis based on the ADE model shows

that, under the condition of constant volume of the GUV, the shape changes as follows: as ΔA_0 increases, prolate $\rightarrow$ pear $\rightarrow$ two-spheres-connected by a narrow neck. These shape changes are the same as those induced by Lfcin B in the PG/PC (1/4)-GUVs (Figure 2.8). This analysis therefore indicates that the interaction of Lfcin B with a GUV increased ΔA_0 of the GUVs. It was hypothesize that A_0^{in} of the GUV does not change. Therefore we can reasonably consider that the binding of Lfcin B induces an increase in the area of the outer monolayer A_0^{out}. Moreover, the observed reversibility of the Lfcin B-induced shape change indicates that the binding of Lfcin B to the membrane interface is reversible.

2.3.9. Association of PG/PC (1/1)-LUVs by Lfcin B

To examine the interaction of PG/PC (1/1) membranes with Lfcin B, I used DLS to determine a time course of the LUV sizes. I used PG/PC (1/1)-LUVs with diameters of 115 nm (Z-average) in buffer A. After mixing with various concentrations of Lfcin B solution (final concentration from 0.50 to 1.0 µM), the average LUV diameter increased with time (Figure 2.9). At 13 min after the mixing, the Z-average values of the LUV suspensions containing 1.0 µM and 0.50 µM LfcinB were 246 nm and 183 nm, respectively. At concentrations of ≤0.20 µM Lfcin B, no significant increase in LUV diameter was observed. After 100 fold dilution of these LUV suspensions with the buffer, Z average values of the suspensions for 1.0 µM and 0.50 µM LfcinB decreased to 118 nm, which is almost the same as the initial diameter of the LUVs (115 nm). This result indicates that LfcinB-induced increase in the size of LUVs are almost reversible. This result can be compared with that of Figure 2.3A because lipid concentrations in both experiments were similar (i.e., 25 and 38 µM in the experiments shown in Figure
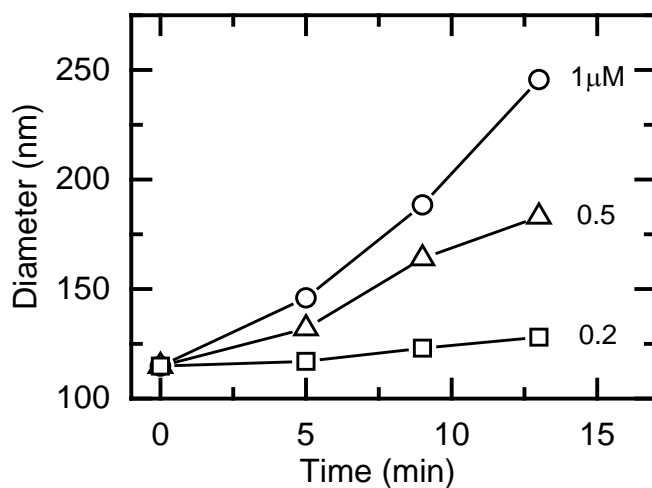
Figure 2.9

Figure 2.9: Time course of the average particle diameter (Z-average) in the LUV suspension. Various concentrations of Lfcin B solution were mixed with PG/PC (1/1)-LUV suspension at $t = 0$. Final Lfcin B concentration is described at the right of each curve. Final lipid concentration was 38 μM. The size distributions were obtained using the non-negative least squares method.

2.3A and B, respectively). Notably, 0.50 μM Lfcin B (i.e., peptide/lipid ratio, P/L, equals to 0.020) did not induce leakage of calcein (Figure 2.3A), nonetheless 0.50 μM Lfcin B (i.e., P/L = 0.013) increased the average LUV diameter (Figure 2.13). Generally the increase in the size of LUVs occurs due to associations of LUVs and membrane fusions of LUVs.

It is considered that the first stage of most membrane fusions is association of LUVs and the second step is the fusion between the associated LUVs. In most cases the association is reversible, i.e., if we decrease the concentration of substances inducing the association, the LUVs are separated each other (Yamazaki et al., 1990). For the second step (i.e., membrane fusion), another factor or longer time is required. The above results of the dilution of the samples indicated that the increase in LUV diameter is due to mostly reversible association of LUVs and partly fusion of LUVs. This is consistent with the result of the reversible binding of LfcinB to the GUV membrane indicated by the experiments of the shape change of the GUVs. Therefore, the results in Figure 2.9 indicates that after the interaction of Lfcin B with LUV membranes, the LUVs associated each other and thus the average size of the LUVs increased with time. The rate of the association increased with an increase in Lfcin B concentration.

2.4. General Discussions

The results of SYTOX green experiments suggest that the Lfcin B-induced damage of *E. coli* plasma membrane to cause membrane permeabilization of SYTOX green is a main cause of death of *E. coli*. The mechanism of the bactericidal activity of Lfcin B is still controversial. Some researchers have suggested that Lfcin B enters the bacterial cytoplasm via translocating plasma membrane, in a manner like that of cell-penetrating peptides, and then acts on DNA, which is a main cause of Lfcin B's

bactericidal activity (see the detailed discussion later) (Bellamy et al., 1992). However, the above results of SYTOX green experiments directly indicate that the Lfcin B-induced damage of the plasma membrane is more plausible for the mechanism of bactericidal activity than the above hypothesis. To elucidate the mechanism of the Lfcin B-induced damage of plasma membrane, it is indispensable to examine directly membrane damage by Lfcin B and to confirm the target of Lfcin B. For this purpose, the interaction of Lfcin B with the LUVs of pure lipid membranes were investigated. The results showed that Lfcin B induced leakage of calcein from the inside of the LUVs, indicating damage of membrane structure of the LUVs. However, there are many causes for the leakage and it is difficult to identify its cause based on the results of the LUV suspension method (Yamazaki, 2008). To clarify the cause of Lfcin B-induced leakage of calcein from the LUVs, the single GUV method was used (Yamazaki, 2008; Islam et al., 2014), to investigate the interaction of Lfcin B with calcein-containing PG/PC-GUVs. It was observed that a rapid leakage of calcein from a GUV started stochastically; its statistical analysis provided a rate constant for Lfcin B-induced pore formation, k_P. After the leakage, the spherical GUV structure remained, but its diameter decreased a little. To elucidate this structural change in the GUVs, the process of the structural change of single GUVs using phase-contrast microscopy were investigated. I observed a rapid efflux of sucrose solution from the inside the GUV, which completed less than 66 ms. This result revealed that Lfcin B induced local rupture in the single GUVs, and from the statistical analysis I obtained the rate constant of local rupture, k_L. The values of k_L and k_P against Lfcin B concentrations were the same within an experimental error. Based on these results, it is concluded that the leakage of calcein from single GUVs occurred as a result of local rupture in the GUVs, and that smaller pores inducing leakage of calcein were not formed before local rupture.

41

In this chapter, the word of "local rupture" was used to express the rapid leakage of sucrose. So far several words have been used to explain such a rapid leakage of internal contents such as sucrose and calcein; large pore formation, local rupture, burst of membranes, and rupture of vesicles (Tamba et al., 2007). However, in many cases of substance-induced rapid leakage of internal contents, its elementary processes have not been well revealed due to the limited time-resolution of the experimental systems, and its mechanisms are not well understood. One exception is the external tension-induced rupture of a GUV (after the rupture, the spherical structure of the GUV completely disappeared (Evans et al., 2011). In this case, a part of elementary processes have been successfully revealed (Evans et al., 2011) and the classical theory (Karal et al.,2015) can explain reasonably that the rupture occurs due to the tension-induced pore formation as follows. Thermal fluctuation in the lateral density of a lipid membrane induces a pre-pore. If the radius of a pre-pore is less than the critical radius, r_a (= Γ/σ), it closes quickly. However, if the radius expands and reaches r_a, the pre-pore transforms into a pore, and then the radius of the pore becomes infinity rapidly, and hence the rupture of the GUV occurs. It is note that the tension-induced rupture of a GUV occurs due to a rapid, large pore formation in lipid membranes. In the case of LfcinB-induced pore formation, we could not observe any processes because the local rupture occurred within 33 ms. Further experiments are indispensable to reveal its elementary processes and its mechanism of the Lfcin B-induced local rupture. After that this phenomena can be more adequately.

As shown in Figure 2.5, during local rupture in a GUV, large structural changes occurred rapidly in the GUV; the diameter of the GUV decreased, and a large area of thicker membrane with higher contrast and several small high-contrast (black) particles appeared on the GUV membrane. On the other hand, Lfcin B can induce association of

PG/PC membranes due to the electrostatic attraction between the positively-charged Lfcin B and the negatively-charged PG/PC membranes, which was supported by the results shown in Figure 2.9. During the local rupture, association of membranes of the GUV may form multilayers locally, which may induce formation of a large area of the thicker membrane region with higher contrast and a small high-contrast (black) particle at several places on the GUV membrane. This model can explain the decrease in the area of the GUV membrane that is indicated by the decrease in GUV diameter. On the other hand, when the interaction of EGCg was investigated, one of antibacterial substances, with single GUVs, it was observed similar rapid leakage of calcein and sucrose, and after the leakage spherical GUVs were not remained, instead the GUV converted to a small lump. In this case it was succeed in observing the evolution of a large pore in the GUV membrane (i.e., the instantaneous pore formation and the following decrease in the radius of the pore). After the formation of a large pore, the high-contrast (black) particles or the thick membrane regions appeared on the GUV membrane, and then during the evolution of the pore with a concomitant of the conversion of the GUV to a small lump, the amount of the high-contrast particles increased. The results using the small-angle X-ray scattering (SAXS) indicated that EGCg induced strong attraction of two bilayers and close contact of them at high concentrations of EGCg (Tamba et al., 2007). Therefore it is clear that the high-contrast (black) particles are formed due to the EGCg-induced attraction of two bilayers after the large pore formation.

To elucidate the mechanism of Lfcin B-induced pore formation, the effects of the electrostatic interactions on the Lfcin B-induced pore formation were investigated. The rate constants of Lfcin B-induced pore formation in PG/PC (1/1)-GUV were much larger than those in PG/PC (1/4)-GUV. The initial process of the binding of Lfcin B to the surface of lipid membranes is controlled by the electrostatic interaction between

43

highly positively charged Lfcin B and negatively charged lipid membranes. It is reasonably expected that the surface concentration of Lfcin B in PG/PC (1/1)-GUV is larger than that in PG/PC (1/4)-GUV. Thus, the results shown in Figure 2.11 indicate that the surface concentration of Lfcin B is one of the key factors for pore formation; with an increase in the surface concentration of Lfcin B, the rate constant of Lfcin B-induced pore formation increases. This tendency has been proved experimentally in the case of magainin 2 (Tamba et al., 2009). Based on the structure of Lfcin B in aqueous solution (as determined by NMR), Lfcin B forms an amphipathic antiparallel β-sheet; the face containing amino acids with high interfacial hydrophobicity (Wimley et al., 1996) (such as F1, W6, W8, L13, and F25) is expected to interact strongly with the membrane interface if Lfcin B lies in parallel with the membrane surface. Experimental results using quenching of Trp fluorescence indicate that the Trp residues of Lfcin B locate at the membrane interface (Schibli et al., 2002) suggesting that Lfcin B indeed lies in parallel with the membrane surface. This strong interaction of Lfcin B with the lipid membrane interface is postulated to induce an increase of the area of the outer monolayer of a GUV, which is supported by the results of Lfcin B-induced shape change (Figure 2.12). It is inferred that this interaction plays an important role in pore formation.

It is important to compare the results of Lfcin B-induced membrane permeation with those of other AMPs and other antimicrobial substance-induced membrane permeation. Magainin 2 initially induced a large, transient pore in lipid membranes following which the radius of the pore decreased to a stable smaller size (Tamba et al., 2007), but the diameter of GUVs did not change significantly after magainin 2-induced pore formation (Tamba et al., 2010). For example, high concentrations of magainin 2 induced a small amount (~10% of the total amount) of leakage of TRD-70k only at the initial stage; at

the final steady-state, the radius of the magainin 2-induced pore was smaller than 2.8 nm (Tamba et al., 2010). In contrast, Lfcin B induced complete leakage of TRD-70k (Figure 2.6). Therefore it can be concluded that the size of the Lfcin B-induced pore is larger than that induced by magainin 2. On the other hand, gomesin, another AMP, induced bursting of GUVs; the structure of GUVs were not observed after the bursting occurred (Domingues et al., 2010). The authors of that report used the "carpet model" to explain the gomesin-induced disruption of the membrane (Pouny, 1992). Similarly, EGCg induced bursting of GUVs; after such bursting, only a small lump (and not a spherical structure) was observed (Tamba et al., 2007). With Lfcin B, spherical GUVs (of reduced diameter) were observed after local rupture, suggesting that the mode of damage of lipid membranes due to Lfcin B is different from that of gomesin and EGCg. However, currently we do not know the mechanism of Lfcin B-mediated local rupture and vesicle bursting. Thus it is difficult to further contrast the differences in membrane damage caused by these various agents.

As discussed above, some researchers consider that the interaction of Lfcin B with DNA is a main cause of Lfcin B's bactericidal activity (Bellamy et al., 1992). Indeed, lactoferrin has been reported to enter cells and interact with DNA (Kanyshova et al., 1995; He et al., 1995). However, it is important to note that even if the main target of an AMP is the plasma membrane of bacteria, the AMP can pass through the induced membrane pore to enter a cell only when the size of the AMP-induced pore is larger than that of the AMP itself. Recently, entry of AMPs into cells by this mechanism was experimentally proved for magainin 2 (Tamba et al., 2007). However, the evidence for the entry of peptides/proteins into cells and their binding to DNA does not necessarily indicate that the binding of peptides/proteins to DNA is the main source of bactericidal activity. Notably, some researchers consider that the damage of plasma membrane due

45

to the interaction of Lfcin B with the lipid membrane region is the primary mechanism of this peptide's bactericidal acitivity. The results in the present report provide direct experimental evidence to support the latter mechanism. At present, we do not have detailed experimental data to propose the mechanism of the Lfcin B-induced local rupture, but changes in the physical properties of the membrane (such as tension due to high surface concentration of Lfcin B) may play a key role in local rupture. The results of Figure 2.7 indicates that LfcinB can induce pore formation even if the surface charge density is lower (i.e., 20mol% DOPG). As described in the Introduction, one of the places where Lfcin B molecules attack bacteria is the mammal stomach. The pH of solution in the stomach is very low (~pH 1−3) (Guyton A.C., 2006), and the pK of PG is ~pH 3 (Cev Hence more than a half of PG molecules are protonated (i.e., the surface charge density of plasma membrane of bacteria becomes less than a half of that at neutral pH) in the stomach. Lfcin B does not have negatively-charged amino acid residues, and hence its charge density does not change in the stomach. Therefore, it can reasonably considered that LfcinB has an antibacterial activity in the stomach.

2.5. Conclusion

In this chapter, evidence for Lfcin B-induced rapid damage of the plasma membrane of *E. coli* was provided. Lfcin B induced leakage of calcein from LUVs and GUVs composed of PG/PC membranes, showing direct evidence that Lfcin B caused a damage of these lipid membranes. Using the single GUV method, it was observed that Lfcin B induced the rapid leakage of calcein and TRD-70k from single GUVs. After the rapid leakage, the spherical shape of the GUV remained although its diameter decreased a little, and the GUV membrane contained a large area of thicker membrane region with higher contrast and several small high-contrast particles. At the time resolution of 33 ms,

the detailed structural changes of the GUV during the rapid leakage were not revealed. The surface concentration of Lfcin B and the associated physical changes in the membrane, such as stretching of membranes, are among the key factors contributing to pore formation. These results indicate that Lfcin B-induced rapid damage of the plasma membrane of *E. coli* with its concomitant rapid leakage of internal contents is a key factor for the peptide's bactericidal activity.

CHAPTER   3

___

Entry of Lfcin B (4-9) into GUVs and *E.coli* without leakage of internal content

3. 1. INTRODUCTION

As described in chap. 1, shorter fragments of LfcinB also have an antimicrobial activity and the interactions of these peptides with lipid membranes have been investigated using various biophysical techniques (Tomita et al., 1994; Kang et al., 1996; Rekdal et al., 1999; Wakabayashi et al., 1999; Strom et al., 2000 Schibli et al., 2002; Strom et al., 2002; Wakabayashi et al., 2003; Nguyen et al., 2005; Jing et al., 2006). However, the elementary processes of the interaction of these LfcinB fragments with lipid membranes and bacteria and also the mechanisms of antimicrobial activity of these shorter segments of LfcinB have not been well understood. In this chapter, I examined the mechanism of the antimicrobial activity of shorter segments of LfcinB (4-9) composed of 6 amino acid residues with the sequence of RRWQWR, which is one of the highest antimicrobial activity among the shorter fragments (Tomita et al., 1994). First I examined the interactions of LfcinB (4-9) and lissamine rhodamine B red-labeled LfcinB (4-9) (i.e., Rh-LfcinB (4-9)) with *E. coli*. The results indicated that Rh-LfcinB (4-9) entered the cytoplasm without damage in the plasma membranes of *E. coli*. To elucidate the elementary processes of the entry of Rh-LfcinB (4-9), I investigated the interactions of Rh-LfcinB (4-9) with single GUVs composed of negatively charged DOPG and electrically neutral DOPC mixtures using the single GUV method for cell-penetrating peptides (CPPs) (Islam et al., 2014; Sharmin et al., 2016). Based on the results, I discussed the mechanism of the antimicrobial activity of LfcinB (4-9) and its translocation across the lipid membranes.

3.2. MATERIALS AND METHODS

3.2.1. Materials

DOPC and DOPG were purchased from Avanti Polar Lipids Inc. (Alabaster, AL). Bovine serum albumin (BSA) and Luria-Bertani (LB) medium contained Bacto peptone, beef extract, and agar were bought from Wako Pure Chemical Industry Ltd. (Osaka, Japan). Alexa Fluor 647 (AF647) and acetoxymethyl (AM)-Calcein were bought from ThermoFisher Scientific (Waltham, MA). Lissamine rhodamine B Red (LRB Red) succinimidylester was purchased from AAT Bioquest Inc. (Sunnyvale, CA). *E. coli* (JM-109) was gifted from Prof. Taketomo Fujiwara, Department of Biological Science, Shizuoka University, Shizuoka, Japan.

LfcinB (4-9) was prepared by the FastMoc method using a 433A peptide synthesizer (PE Applied Biosystems, Foster City, CA). The sequence of LfcinB (4-9) (6-mer) is RRWQWR, which has an amide-blocked C terminus. The fluorescence probe rhodamine-labeled LfcinB (4-9) (Rh-LfcinB (4-9)), which has one fluorophore Rh at the N-terminus of the peptide, was synthesized using a standard method (Islam et al., 2014) by the reaction of LRB Red succinimidylester (20 mg) with LfcinB (4-9)-peptide resin (80 mg) (molar ratio of reagent to peptide: 1.1 to 1) in dimethylformamide for 24 h at room temperature. Rh-LfcinB (4-9) was cleaved from the resin using trifluoroacetic acid (TFA), 1, 2-ethanedithiol, thioanisole, and MilliQ water (10/0.25/0.5/0.5, volume ratio) and phenol (0.15 g per 2 mL TFA). The method for purification of the peptide was described previously (Masum et al., 2003). Mass spectra of LfcinB (4-9) and Rh-LfcinB (4-9) were acquired by LC−MS analysis using the linear ion trap time-of-flight mass spectrometer (LIT–TOF MS), NanoFrontier eLD (Hitachi High-Technologies Corporation, Tokyo, Japan) as previously described (Moniruzzaman et al., 2015). The samples were separated by a MonoCap C18 Fast-flow column (0.05 mm ID x 150 mm long; GL Sciences, Inc., Tokyo, Japan) and ionized with a nano-electrospray ionization source, and then mass spectra were obtained in the positive ion mode at scan mass range m/z

200–2000. The measured masses of LfcinB (4-9) and Rh-LfcinB (4-9) were 985.56 ± 0.01 and 1636.78 ± 0.01 Da, respectively, which correspond to the molecular masses calculated from the monoisotopic mass of all the atoms in these molecules.

LfcinB (4-9) concentrations in buffer were determined by absorbance using the molar extinction coefficient of Trp at 278 nm (i.e., 5,500 $M^{-1}cm^{-1}$). LfcinB (4-9) has two Trp residues and hence the molar extinction coefficient of LfcinB (4-9) is 11,000 $M^{-1}cm^{-1}$. On the other hand, Rh-LfcinB (4-9) concentrations in buffer were determined by absorbance using the molar extinction coefficient of Rh at 568 nm (i.e., 95,000 $M^{-1}cm^{-1}$).

3.2.2. Measurement of minimum inhibitory concentration (MIC)

The same method described in section 2.2.3 was used.

3.2.3. LfcinB (4-9)-induced entry of SYTOX green into cytoplasm of *E. coli*

The same method described in section 2.2.4 was used.

3.2.4. Investigation of the interactions of Rh-LfcinB (4-9) with single *E. coli* containing calcein using confocal microscopy

An *E. coli* suspension was subcultured on nutrient agar plates at 37 °C for overnight to get single colonies. A single colony of bacteria was then grown in nutrient broth medium (1 colony/2mL nutrient media) for 6 to 7 h (exponential phase cells). The bacterial suspension was 10 times diluted to a final bacterial concentration of 1×10^{6} CFU/mL, which was pelleted by centrifugation (350 × g, 10 min, H-18F) and the pellet was washed using fresh media. For loading calcein in *E. coli*, the method of Dubey et al. (2011) was used. 50 µL of AM-calcein (1µg/µL in DMSO solution) was added into 1 mL of the bacterial suspension, which was shaken using a rotary shaker for 2.3 h at room temperature under dark condition. Then the

suspension was centrifuged at $350 \times g$ for 10 min, and the pellet was resuspended in fresh, dye free LB medium. This procedure was repeated twice, and finally the suspension was resuspended in buffer A. Interactions of peptides with *E. coli* containing calcein were observed using a confocal laser scanning microscope (CLSM) (FV-1000, Olympus, Tokyo, Japan) at 25 ± 1 °C with a stage thermocontrol system (Thermoplate, Tokai Hit, Shizuoka, Japan). For CLSM measurements, fluorescence images of calcein (473 nm laser) were obtained using a $60\times$objective (UPLSAPO060X0, Olympus) (NA = 1.35) (Islam et al., 2014). During the interaction of peptides with a single cell of *E. coli,* various concentrations of Rh-LfcinB (4-9) in buffer A were added continuously to the neighborhood of the *E. coli* through a 20-µm-diameter glass micropipette positioned by a micromanipulator (Karal et al., 2015). The distance between the *E. coli* and the tip of the micropipette was 50–60 µm.

3.2.5. GUV preparations

GUVs of DOPG/DOPC (1/1; molar ratio) membranes (i.e., PG/PC (1/1)-GUVs) were prepared by incubation of buffer A containing 0.1 M sucrose and 1 mM calcein or 6 µM AF647 with dry lipid films by the natural swelling at 37 °C for 2−3 h (Islam et al., 2014). I prepared GUVs containing small vesicles inside the GUV lumen according to the method described in our previous paper (Islam et al., 2014). The membrane filtering method was used to remove untrapped fluorescent probes (Tamba et al., 2011). Purified GUV suspension (0.1M sucrose and 0.1M glucose in buffer A as the internal solution and the external solution, respectively) was transferred into a hand-made microchamber (Yamazaki, 2008). To prevent strong interaction between the glass surface and GUVs, the inside of the microchamber was coated with 0.10 % (w/v) BSA in the same buffer for the experiments (Yamazaki, 2008; Karal et al., 2015).

3.2.6. Investigation of the interactions of LfcinB (4-9) with single GUVs containing calcein

Various concentrations of LfcinB (4-9) solution in buffer A containing 0.10 M glucose were continuously added in the vicinity of a GUV through a ~20-µm-diameter glass micropipette positioned using a micromanipulator. The distance between the GUV and the tip of the micropipette was ~70 µm, and the applied pressure, ΔP ($= P_{in} - P_{out}$, where P_{in} and P_{out} were the pressure of the inside and the outside of a micropipette, respectively) was 30 Pa (Karal et al., 2015). Phase-contrast and fluorescence images of GUVs were recorded using a high-sensitivity EM-CCD camera (C9100-12, Hamamatsu Photonics K.K., Hamamatsu, Japan) with a hard disk. Three ND filters were used to decrease the intensity of the incident light, resulting in conditions where almost no photobleaching of fluorescent probes in a GUV occurred during the interaction of the LfcinB (4-9) solution with single GUVs. Thus, under these conditions, the decrease in fluorescence intensity inside a GUV corresponded to leakage of the fluorescent probes from the inside to the outside of the GUV. The fluorescence intensity inside the GUVs was determined using the AquaCosmos software (Hamamatsu Photonics K.K.), and the average intensity per GUV was estimated. The details of this method were described in our previous reports (Yamazaki, 2008; Karal et al., 2015).

3.2.7. Investigation of the interactions of Rh-LfcinB (4-9) with single GUVs containing AF647

The single GUV method for investigations of cell penetrating peptides (CPPs) (Islam et al., 2014) was used. GUVs were observed using the CLSM at 25 ± 1 °C using the stage thermocontrol system. Fluorescence images of GUVs due to AF647 (635 nm laser) and
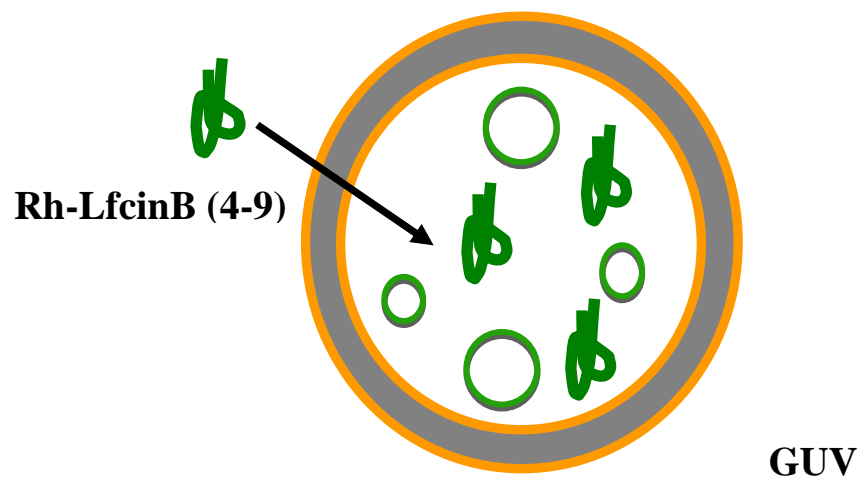
Figure 3.1: A schematic diagram of interaction of Rh-LfcinB (4-9) with GUVs.

Rh-LfcinB (4-9) (559 nm laser) were obtained using the 60× objective (Karal et al., 2015). Interactions of Rh-LfcinB (4-9) with a single GUV were investigated by adding various concentrations of Rh-LfcinB (4-9) in buffer A containing 0.1 M glucose continuously to the neighborhood of the GUV using a 20-µm-diameter glass micropipette (Fig.3.1). The time course of the fluorescence intensity of GUVs was analyzed according to paper of Islam et al. (2014).

3.3. RESULTS AND DISCUSSION

3.3. 1. MIC of Lfcin B (4-9) against *E. coli*

First the antimicrobial activity of the Lfcin B (4-9) was investigated. Using the standard method, it was determined the MIC of Lfcin B (4-9) against *E. coli* (JM-109) as 25 ± 10 µM.

3.3.2. Lfcin B (4-9)-induced influx of SYTOX green into cytoplasm of *E. coli*

To clarify the target of the bactericidal activity of Lfcin B (4-9) against *E. coli*, permeabilization of the plasma membrane of *E. coli* was investigated by measuring the influx of the membrane-impermeant fluorescent probe, SYTOX green, into the bacterial cytoplasm (Roth et al., 1997; Mukherjee et al., 2014). Notably, the fluorescence of SYTOX green is elevated upon binding to nucleic acids; thus increased fluorescence intensity indicates influx of the marker into the cytoplasm. As shown in Figure 3.2, the fluorescence intensity of SYTOX green did not increase significantly with time during the incubation of SYTOX green with an *E. coli* suspension in the presence of 100 and 250 µM Lfcin B (4-9). In contrast as describe in chapter 2, 50 µM Lfcin B induced an

Figure 3.2.

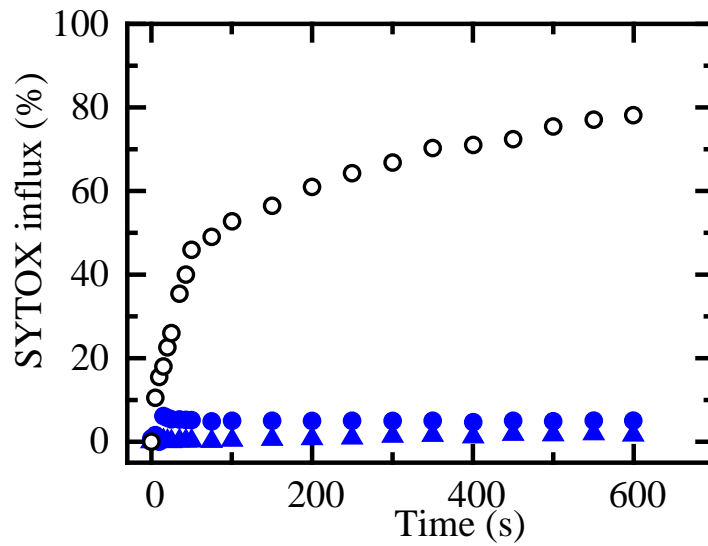Figure 3.2: Time course of influx of SYTOX green into cytoplasm of *E. coli*. Time courses of fluorescence intensity of SYTOX green are shown during the interaction of various concentrations of Lfcin B (4-9) with *E. coli* suspension at 25 °C. (▲) 100 μM, and (●) 250 μM Lfcin B (4-9). Bacteria density was 1×10^6 CFU/mL. For comparison, the data for 50 μM Lfcin B (○) is shown, which is the same as Fig. 2 .1 in chapter 2.

increase in the fluorescence intensity of SYTOX green and 80 % SYTOX influx was observed at 10 min (Figure 3.2).

The results of Figure 3.2 indicate that during the interaction of *E. coli* with Lfcin B (4-9) its plasma membrane was not damaged and as a result SYTOX green did not enter the inside of *E. coli*., which is contrast with the results of LfcinB that the plasma membrane of *E. coli* was rapidly damaged and as a result SYTOX green permeabilized through the plasma membrane to enter the inside of *E. coli*. These results suggests that bactericidality due to LfcinB (4-9) does not reflect the damage of *E. coli* plasma membrane.

3.3.3. Induction of calcein leakage from PG/PC (1/1)-GUVs by Lfcin B (4-9)

To elucidate the interaction of Lfcin B (4-9) with plasma membrane of *E. coli*, I investigated the interaction of Lfcin B (4-9) with single PG/PC (1/1)-GUVs containing calcein and 0.10 M sucrose using the single GUV method (Islam et al., 2014; Yamazaki, 2008). During observation of a single GUV in buffer A containing 0.10 M glucose at 25°C by phase-contrast fluorescence microscope, the tip of a micropipette was approached to the GUV at $t = 0$ and the Lfcin B (4-9) solution was continuously added from the micropipette into the neighborhood of the GUV. First the interaction of 50.0 μM Lfcin B (4-9) with a single GUV was investigated. Prior to Lfcin B (4-9) addition, a phase-contrast microscopic image of the GUV indicated a high contrast in the GUV (Figure 3.3A-1) due to the difference in the saccharide concentrations between the inside (0.10 M sucrose) and the outside (0.10 M glucose) of the GUV. A fluorescence microscopic image of the same GUV (Figure 3.3A-2) showed a high concentration of calcein inside the GUV at this time. After starting the addition of the 50.0 μM solution of Lfcin B (4-9), the fluorescence intensity inside the GUV was not change during the

56

Figure 3.3.

(A)
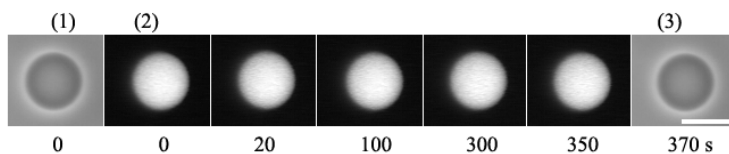
(B)
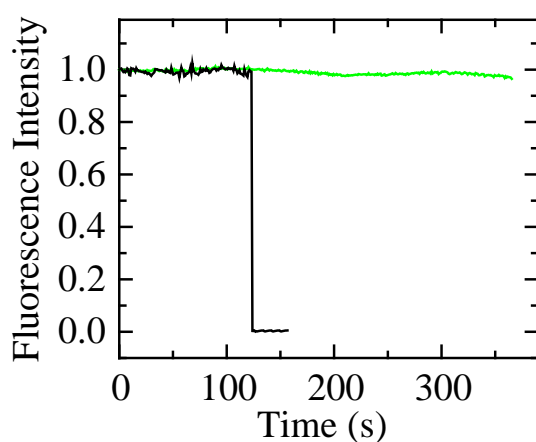
Figure 3.3: Membrane permeation of calcein from single PG/PC (1/1)-GUVs induced by Lfcin B (4-9). (A) Leakage of calcein from single PG/PC (1/1)-GUVs was induced by 50.0 μM Lfcin B (4-9) in buffer A at 25°C. Fluorescence images (2) show that the calcein concentration inside the GUV remained constant after the addition of Lfcin B (4-9. The numbers above each image show the time in seconds after the Lfcin B (4-9) addition was started. Also shown are phase contrast images of the GUV at time 0 (1) and 149 s (3). The bar corresponds to 20 μm. (B) Time course of the change in the normalized fluorescence intensity of the GUV shown in (A) (green line). The normalized fluorescence intensity of the intact GUV before the initiation of the membrane permeation as 1.0. For comparison, the data for 5 μM Lfcin B (black line) is shown, which is the same data of Fig. 2.4 (B) in chapter 2.

interaction (up to 6 min) (Figure 3.3A-2, 3.3B). After 370 s a phase-contrast image of the same GUV was the same as before the interaction (Figure 3.3A-3). When the same experiments were carried out using 20 single GUVs, the same results were obtained. These results indicate that Lfcin B (4-9) could not induce pore formation in PG/PC (1/1)-GUVs nor rupture of these GUVs. This is highly contrast with the result of LfcinB; in this case a rapid leakage occurred (see an example of 5.0 µM Lfcin B in Figure 2.3 B; this is the same data as Fig. 2.4) These results support the results of entry of SYTOX green: Lfcin B (4-9) could not induce any damages in *E. coli* plasma membrane, whereas LfcinB induced damage in its plasma membrane.

3.3.4. Entry of Rh-LfcinB (4-9) into a single *E. coli*

The above results indicate that bactericidality due to LfcinB (4-9) is not due to the damage of *E. coli* plasma membrane. Hence it can be expected that entry of this peptide into cytoplasm of *E. coli* to bind DNA or other proteins causes the bactericidality. To examine the activity of LfcinB (4-9) to enter cytoplasm of *E. coli*, I investigated the interaction of a fluorescent probe-labeled LfcinB (4-9) (Rh-LfcinB (4-9)) with a single cell of *E. coli* containing calcein using CLSM. First the interaction of 5.0 µM Rh-LfcinB (4-9) with a single cell of *E. coli* was investigated in buffer A at 25°C. The Rh-LfcinB (4-9) solution was continuously provided to the neighborhood of the *E. coli* through a micropipette, so the Rh-LfcinB (4-9) concentration near the *E. coli* became constant at the steady state, which was almost the same as that in the micropipette (Karal et al., 2015). During the interaction of 5.0 µM solution of Rh-LfcinB (4-9), the fluorescence intensity of calcein in the *E. coli* did not change during the experiment (up to 10 min) (Figure 3.4A, B and green lines in Figure 3.4C, D), indicating no pore formation in plasma membrane through which calcein leaked. There were two types of times causes of the FI

Figure 3.4

(A)

(B)

(C)

(D)
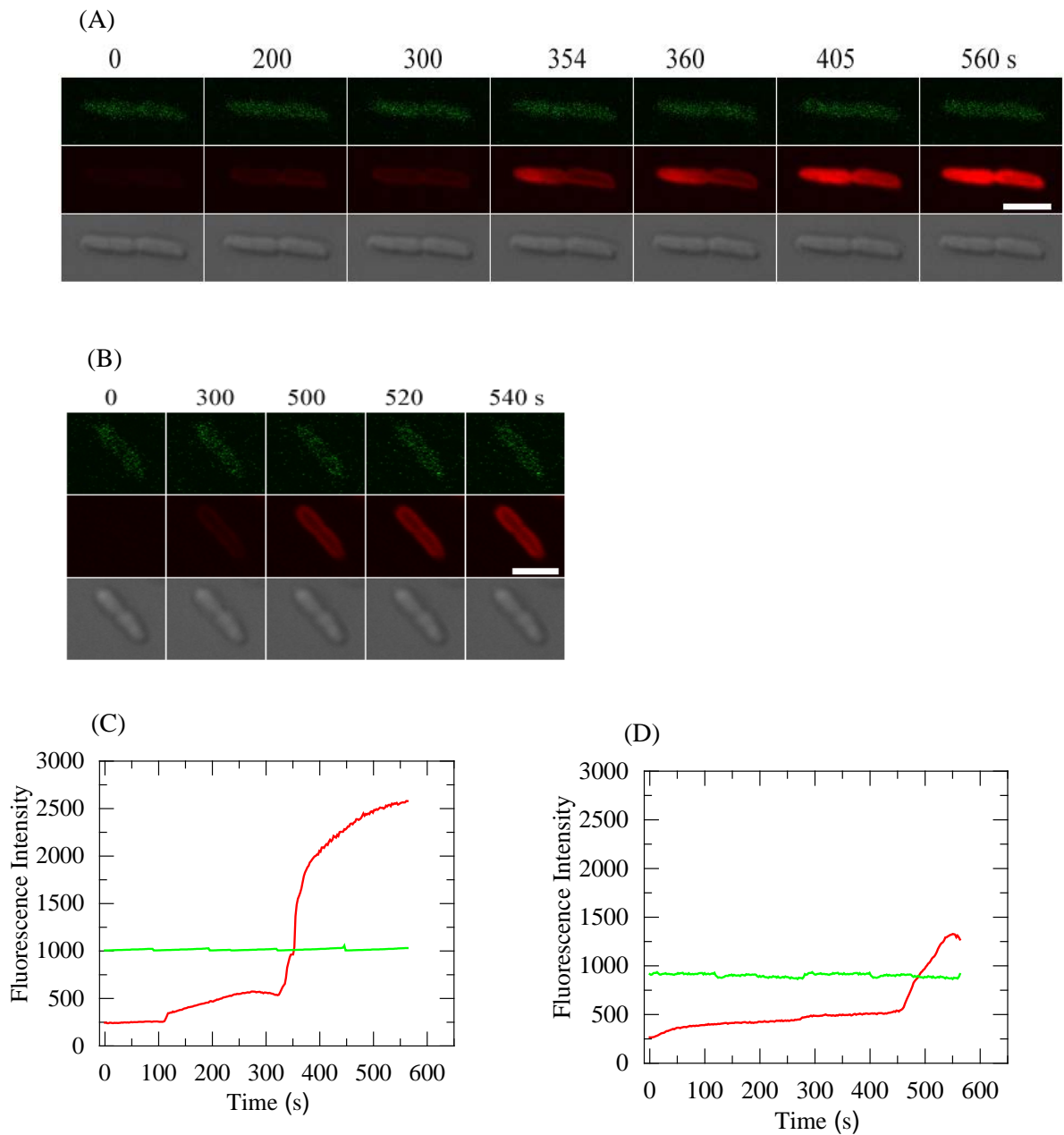
Fig 3.4: Entry of Rh-LfcinB (4-9) into a single *E. coli* cell containing calcein. (A) CLSM images of (1) calcein, (2) Rh-LfcinB (4-9), and (3) DIC. B) CLSM images of (1) calcein, (2) Rh-LfcinB (4-9), and (3) DICThe numbers above each image show the time in seconds after the addition of 5.0 μM Rh-LfcinB (4-9) was started. The bar is 2.0 μm. (C) Change in the fluorescence intensity of the cell of *E. coli* during the interaction of Rh-LfcinB (4-9) over time shown in (A). (D) Change in the fluorescence intensity of the cell of *E. coli* during the interaction of Rh-LfcinB (4-9) over time shown in (B). Green and red lines correspond to the fluorescence intensity of calcein and of Rh-LfcinB (4-9) in the cell of *E. coli*, respectively.

of cytoplasm of *E. coli* due to Rh-LfcinB (4-9), One is that the FI of cytoplasm gradually increased with time to reach a steady value at ~300 s, then rapidly increased after 320 s, and finally the FI of the cytoplasm was similar to that of the rim of *E. coli* (i.e., type A) (Figure 3.4A and red line in Figure 3.4C). Type A of the time course of the FI was observed in 6 cells, which corresponds to 50% of all examined *E. coli* cells (*n* = 12). the other type of time course is that the FI gradually increased with time to reach a steady value at ~ 100 s which remained almost constant for a few minutes, then rapidly increased after 450 s, and finally the FI of the cytoplasm was lower than that of the rim of *E. coli* (i.e., type B) (Figure 3.4B and red line in Figure 3.4D).

It can be considered that type A indicates the Rh-LfcinB (4-9) outside the *E. coli* translocated through the outer membrane of *E. coli* to enter its periplasm, then translocated through *E. coli* plasma membrane to enter its cytoplasm without pore formation, i.e., Rh-LfcinB (4-9) has a cell-penetrating activity against *E. coli*. In type A, the first steady state of FI (i.e., 100~320 s) corresponds to the state of the binding of Rh-LfcinB (4-9) to the outer and the plasma membranes of *E. coli*. On the other hand, type B indicates that the Rh-LfcinB (4-9) outside the *E. coli* translocated through the outer membrane of *E. coli* to its periplasm, but could not enter its cytoplasm.

3.3.5. Entry of Rh-LfcinB (4-9) into a single DOPG/DOPC-GUVs without pore formation

To examine the activity of LfcinB (4-9) to translocate across lipid bilayers, I investigated whether Rh-LfcinB (4-9) can enter single GUVs of lipid bilayers using the single GUV method for investigation of CPPs (Islam et al., 2014). For this aim, I observed using CLSM the interaction of Rh-LfcinB (4-9) with single PG/PC (1/1) GUV containing small vesicles composed of PG/PC (1/1) and AF647 in the GUV lumen. First an interaction of 5.0 μM

Figure 3.5

(A)

(B)

(C)
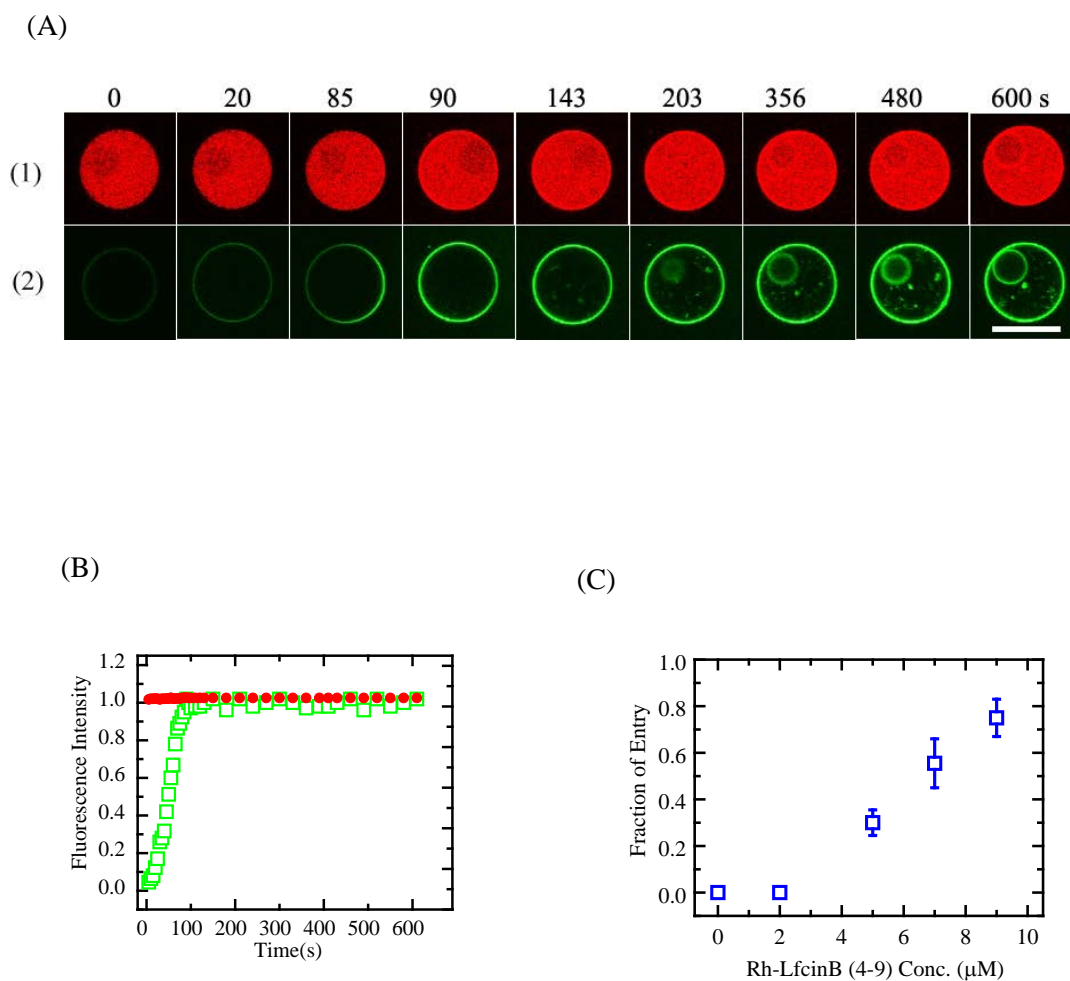
Figure 3.5: Leakage of AF647 and entry of Rh-LfcinB (4-9) into single PG/PC (1/1)-GUVs containing small vesicles, induced by 5.0 µM Rh-LfcinB (4-9). (A) CLSM images of (1) AF647 and (2) Rh-LfcinB (4-9). The numbers above each image show the time in seconds after the addition of Rh-LfcinB (4-9) was started. The bar corresponds to 20 µm. (B) Time course of the normalized rim intensity of the GUV due to Rh-LfcinB (4-9) shown in (A). Red and green points correspond to the fluorescence intensity of AF647 in the GUV lumen and of Rh-LfcinB (4-9) in the rim of the GUV, respectively. (C) Dependence of the fraction of entry of Rh-LfcinB (4-9) without pore formation on the Rh-LfcinB (4-9) concentration.

Rh-LfcinB (4-9) with a single GUV was observed in buffer A containing 0.1 M glucose at 25°C. The Rh-LfcinB (4-9) solution was continuously provided to the neighborhood of the GUV through a micropipette. After starting the addition of the 5.0 μM Rh-LfcinB (4-9), the FI of AF647 in the GUV lumen did not change during the experiment (Figure 3.5A (1) and red solid square in Figure 3.5B), indicating no pore formation in the lipid bilayer through which AF647 leaked. On the other hand, the FI of the GUV membrane (i.e., the rim intensity) due to Rh-LfcinB (4-9) gradually increased and at 100 s it became almost steady, which remained constant during the interaction (Figure 3.5A (2) and green open squares in Figure 3.5B). At initial time of the interaction, there was no FI inside the GUV, but after 142 s, the membranes of the small vesicles inside the GUV emitted fluorescence ($t = 143-600$ s in Figure 3.5A (2)). These results indicate that Rh-LfcinB (4-9) in the aqueous solution outside the GUV translocated through the GUV membrane and entered the GUV lumen without pore formation, then bound to the membrane of the small vesicles. The same experiments were performed using 13 GUVs. The entry of Rh-LfcinB (4-9) into the GUV lumen within 10 min interaction was observed in 4 GUVs, and hence the fraction of entry of Rh-LfcinB (4-9) at 10 min without pore formation, P_{entry} (10 min), was 0.25. To confirm reproducibility, two independent experiments were performed, and similar results were obtained. The mean value and the standard error of P_{entry} (10 min) was 0.31 ± 0.06.

I also examined the concentration dependence of the entry of Rh-LfcinB (4-9) into a GUV without the leakage of AF647. Figure 3.5C shows the Rh-LfcinB (4-9) concentration dependence of P_{entry} (10 min). At Rh-LfcinB (4-9) concentrations of ≤ 2.0 μM, the entry of Rh-LfcinB (4-9) into a GUV was not observed during 10 min interaction. At and above 5.0 μM Rh-LfcinB (4-9), the entry of Rh-LfcinB (4-9) was observed in some examined GUVs, and P_{entry} (10 min) increased with an increase in Rh-LfcinB (4-9) concentration.

Figure 6

(A)

(B)

(C)
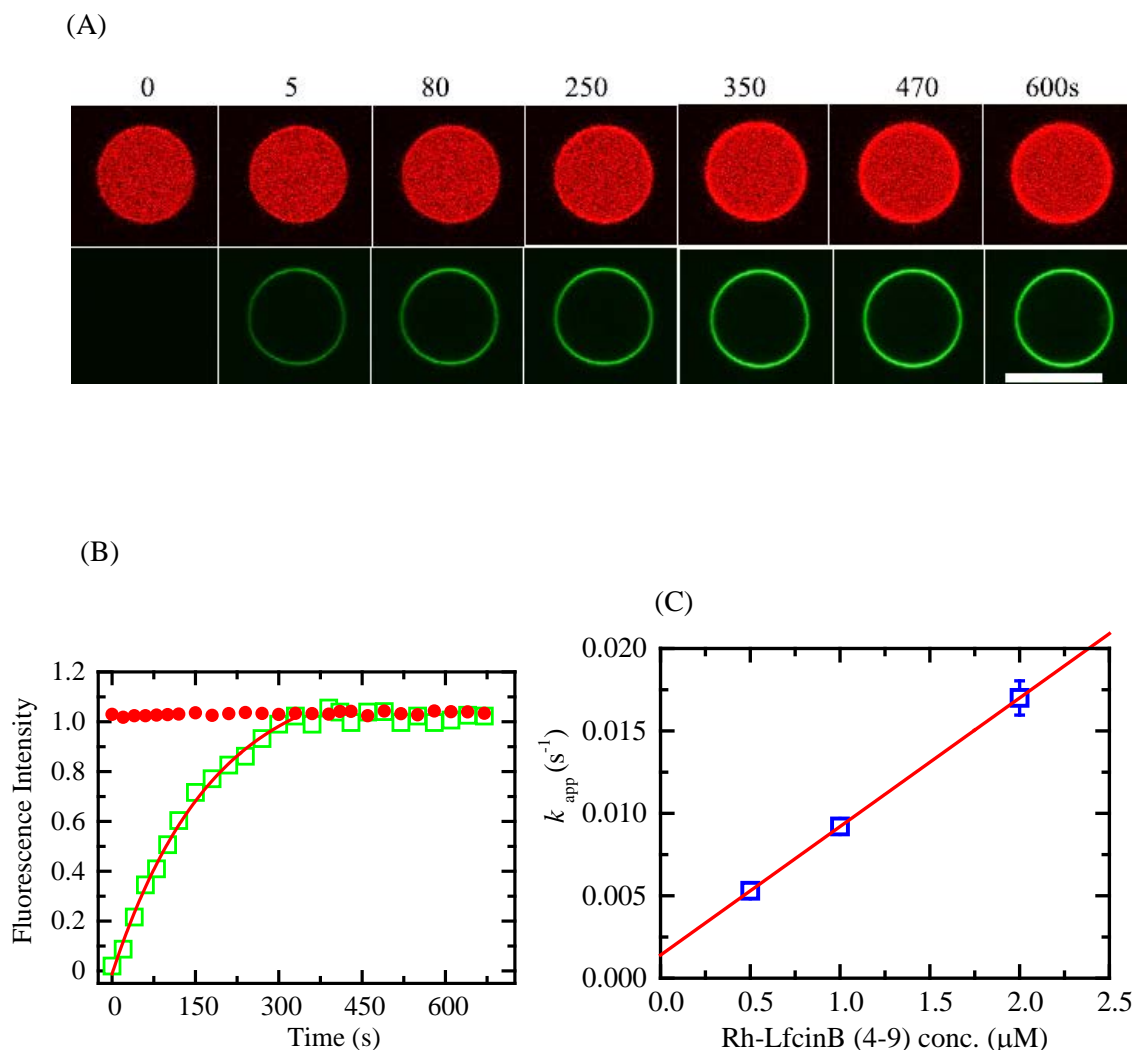
Figure 3.5: Time course of rim intensity due to Rh-LfcinB (4-9) in single PG/PC (1/1)-GUVs not containing small vesicles induced by 1.0 μM Rh-LfcinB (4-9). (A) CLSM images of (1) AF647 and (2) Rh-LfcinB (4-9). The numbers above each image show the time in seconds after the addition of Rh-LfcinB (4-9) was started. The bar corresponds to 20 μm. (B) Time course of the normalized rim intensity of the GUV due to Rh-LfcinB (4-9) shown in (A). Red and green points correspond to the fluorescence intensity of AF647 in the GUV lumen and of Rh-LfcinB (4-9) in the rim of the GUV, respectively. The solid black line represents the best fit curve using eq. 3.1. (C) Dependence of k_{app} on Rh-LfcinB (4-9) concentration. The time course of the rim intensity of 21-22 GUVs was measured (two independent experiments). The mean values and standard errors of k_{app} are shown. The solid red line represents the best fit curve using eq. 3.2.

3.3.6. Translocation of Rh-LfcinB (4-9) from the outer to the inner monolayer in single DOPG/DOPC-GUVs

To elucidate the kinetics of entry of Rh-LfcinB (4-9), next I examined and analyzed the time course of Rh-LfcinB (4-9) concentration in the GUV membrane, $C_M(t)$ [M], using the method developed by Islam et al. (2014). For this purpose, I examined the interaction of Rh-LfcinB (4-9) with a single GUV not containing small vesicles using the same method described in the section 3.3.5, because in the experiments using the GUVs containing the small vesicles in the GUV lumen shown in Figure 3.5A some fluctuations of the intensity of the GUV membrane were caused due to the small vesicles near the GUV membrane (Islam et al., 2014). Since it is difficult to analyze the rapid increase in rim intensity shown in Figure 3.5B (Islam et al., 2014), lower concentrations of Rh-LfcinB (4-9) was used. During the interaction of 1.0 μM Rh-LfcinB (4-9) with a single PG/PC (1/1)-GUVs containing AF647 (Figure 3.6A (1)), a high concentration of AF647 inside the GUV remained essentially constant during the experiment (up to 10 min) (red circles in Figure 3.6B), indicating no leakage of AF647. The rim intensity gradually increased with time and at 350 s was almost steady (Figure 3.6A (2) and green squares in Figure 3.6B). The elementary processes of the entry of CPPs such as TP10 and R$_9$ into single GUVs was previously proposed (Islam et al., 2014; Sharmin et al., 2016) and here I applied the same elementary processes to the entry of Rh-LfcinB (4-9) into a GUV lumen (Figure 3.7). First, Rh-LfcinB (4-9) in the solution outside a GUV binds to the external monolayer of the GUV at its membrane interface, whose rate constant is k_{ON}. Next, Rh-LfcinB (4-9) translocate from the external to the internal monolayer, whose rate constant is k_{FF}, and then unbinds from the internal monolayer into aqueous solution near the GUV membrane (where the Rh-LfcinB (4-9) concentration is C_{in}), whose rate constant is k_{OFF}. Finally, Rh-LfcinB (4-9) diffuses into the GUV bulk lumen, whose rate constant is k_{diff}. It is also necessary to consider the backward reactions. After starting the interaction of Rh-LfcinB (4-9)

Figure 3.7
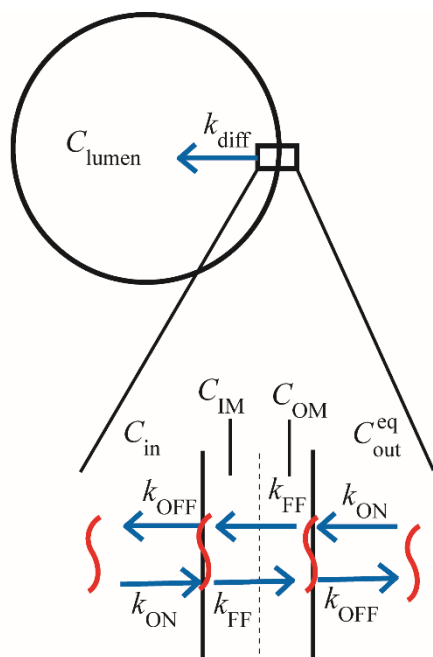
Figure 3.7: Schematic showing the elementary processes for the entry of Rh-LfcinB (4-9). C_{lumen}, C_{in}, a

C_{out}^{eq} are respectively the Rh-LfcinB (4-9) concentration in the GUV bulk lumen, in the GUV lumen

adjacent to the membrane, and in the aqueous solution outside the GUV adjacent to the membrane. C_{OM}

and C_{IM} are the Rh-LfcinB (4-9) concentration in the external and internal monolayer of the GUV,

respectively. k_{ON}, k_{OFF}, and k_{diff} are the rate constants for the binding of Rh-LfcinB (4-9) to the monolayer

of a GUV from aqueous solution, for the unbinding of Rh-LfcinB (4-9) from the monolayer and release

into the aqueous solution adjacent to the membrane, and for the diffusion from the GUV lumen adjacent

to the membrane and into the bulk lumen (i.e., the central region of the GUV). k_{FF} is the rate constant for

the translocation of Rh-LfcinB (4-9) from one monolayer to the other. This figure is reprinted from

Sharmin et al, 2016 with permission from the American Chemical Society.

with a GUV, the Rh-LfcinB (4-9) concentration in the neighborhood of the GUV elevated from zero to a constant, steady value, C_{out}^{eq} [M], for a short time, and remained constant during the interaction of Rh-LfcinB (4-9) with the single GUV (Karal et al., 2015; Sharmin et al., 2016). If the transfer of Rh-LfcinB (4-9) between the external and internal monolayers is fast, i.e., the rate of the transfer is faster than that of binding of Rh-LfcinB (4-9) and faster than that of unbinding from the membrane to aqueous solution. For this case, following equation of Rh-LfcinB (4-9) concentration in the GUV membrane, $C_M(t)$, which is hold for the initial time (i.e., when the Rh-LfcinB (4-9) concentration in the GUV lumen is low) (Karal et al., 2015).

$$C_M(t) = A\,[1 - \exp(-k_{app}t)] \tag{3.1}$$
$$\text{where} \quad k_{app} = k_{ON}C_{out}^{eq}/2 + k_{OFF} \tag{3.2}$$

where k_{app} is the apparent rate constant of the elevation in $C_M(t)$ and A is a constant. The increase in the rim intensity of PG/PC (1/1)-GUVs (Figure 5B) over time was fit well by eq. 3.1 (the black line in Figure 5B) and gave a value for k_{app} of 8.1×10^{-3} s^{-1}. k_{app} increased linearly with increasing C_{out}^{eq} (Figure 5C), and the best fit of this relationship with eq. 3.2 provided values of $k_{ON} = (1.4 \pm 0.1) \times 10^4$ M^{-1}s^{-1} and $k_{OFF} = (2.3 \pm 0.4) \times 10^{-3}$ s^{-1}. Therefore, the binding constant of Rh-LfcinB (4-9) to the membrane, K_B, is determined by $K_B = k_{ON}/k_{OFF}$: hence $K_B = (6 \pm 1) \times 10^6$ M^{-1} for PG/PC (1/1)-GUVs.

3.4. GENERAL DISCUSSION

The above results show that Rh-LfcinB (4-9) entered cytoplasm of a single cell of *E. coli* and lumen of single GUVs without damages of these membranes, indicating that Rh-LfcinB (4-9) is one of CPPs (Magzoub et al., 2004; Zorko et al., 2005; Koren et al., 2012; Stanzi¥l et al.,

2013; Pisa et al., 2015). The cell-penetrating activity of Rh-LfcinB (4-9) increased with an increase in its concentration, and it became large at and above 5.0 μM for 10 min interactions. This concentration range is lower than the MIC value of LfcinB (4-9) may against *E. coli* (JM-109) (i.e., 25 ± 10 μM). If entry of Rh-LfcinB (4-9) may induce death of *E. coli* after some lag time, this result suggests that cell-penetrating activity Rh-LfcinB (4-9) would be higher than that of LfcinB (4-9). This can be explained by the labeling of fluorescent probe (Rh) to the peptide: the attachment of a hydrophobic fluorescent probe affects the behavior the interaction of LfcinB (4-9) with lipid bilayers and increases the cell penetrating activity, which has been suggested in the case of CPPs (Bechara et al., 2013).

For interactions of CPPs with vesicles of lipid membranes, several patterns were reported. The pattern A is the entry of CPPs without leakage of water soluble fluorescent probes such as AF647, i.e., without pore formation in lipid bilayers. Interactions of oligoarginine, R_9, with most lipid membranes belong to this pattern A (Sharmin et al., 2016). In the pattern A, it is considered that translocation of CPPs occurs through transient hydrophilic prepores in the bilayer (Levandy et al., 2013; Karal et al., 2016). The pattern B is the entry of CPPs through pores in lipid bilayers. Interactions of human immunodeficiency virus Tat protein-derived peptide (i.e., Tat peptide) and R_6 with lipid bilayers comprised of dioleoylphosphatidylserine (DOPS) and dioleoylphosphatidylethanolamine (DOPE) belong to this pattern B (Mishra et al., 2008; 2011; Ciobansu et al., 2010). The pattern C is the entry of CPPs before leakage of water soluble fluorescent probes, i.e., before pore formation. Interactions of transportan 10 with most lipid membranes belongs to this pattern C (Karal et al., 2015). In the pattern C, it is considered that translocation of CPPs occurs through transient hydrophilic prepores in the bilayer, and after the translocation pore formation occurs due to another mechanism (Karal et al., 2015). Based on the results in this chapter, the interaction of Rh-LfcinB (4-9) with PG/PC (1/1) membrane

belongs to the pattern A. Therefore, it can be considered that the translocation of Rh-LfcinB (4-9) occurs through transient hydrophilic prepores in the bilayer.

Several studies on the interactions of shorter fragments of LfcinB with lipid membrane have been reported. LfcinB (17-31) and its mutants did not induce significant leakage of calcein from LUVs of various lipid compositions (palmitoyl oleoyl PG (POPG), palmitoyl oleoyl PC (POPC), POPG/POPC (1/1)), but differential scanning calorimetry (DSC) studies indicate that these peptides strongly bind to negatively charged PG membranes (Strom et al., 2002). Most results indicate that these shorter fragments of LfcinB did not damage lipid membranes to induce leakage of internal contents of vesicles. However there are several possibilities of sources of antimicrobial activity. The binding of peptides with lipopolysaccharide (LPS) which locates in the external monolayer of the outer membrane of gram negative bacteria, may be a source of antimicrobial activity (Farnaud et al., 2004). The other possibility for antimicrobial activity is the entry of AMPs into cytoplasm of bacteria to bind DNA or other proteins, which is demonstrated in the case of buforin II (Park et al., 2000). Very recently, it has been reported that a 5-residue linear fragment of LfcinB (i.e., LfcinB (4-8)) can enter human lung cancer A549 cells, (Liu et al., 2016) which supports our conclusion that the short fragments of LfcinB are one of CPPs. Moreover, our results in this report clearly indicate that LfcinB (4-9) can translocate across lipid bilayers and enter GUVs composed of the lipid bilayers without pore formation and also it can enter *E. coli* without damage of its plasma membrane. Therefore, we can reasonably consider that the source of antimicrobial activity of Rh-LfcinB (4-9) is similar to that of buforin II (Park et al., 2000)

3.5. CONCLUSION

In this chapter, it was found that Rh-LfcinB (4-9) translocated continuously across lipid bilayers of single GUVs of pure lipid membranes (i.e., PG/PC (1/1)) and entered their lumens

without pore formation for the first time, to the best of my knowledge. This phenomena is the same as that of oligoarginine such as R$_9$, one of CPPs (Sharmin et al., 2016). I also found that Rh-LfcinB (4-9) entered cytoplasm of *E. coli* without damages of its plasma membranes, indicating that Rh-LfcinB (4-9) has a cell-penetrating activity. The elementary processes of the entry of Rh-LfcinB (4-9) were also revealed; the rate constant of the binding of Rh-LfcinB (4-9) with PG/PC (1/1) bilayer and that of its unbinding from the bilayer to aqueous solution were determined. Based on these results, it can be reasonably considered that Rh-LfcinB (4-9) can translocate through lipid membrane regions of the plasma membrane of *E. coli*. Therefore, the target of LfcinB (4-9) for its antimicrobial activity is not plasma membrane of *E. coli* but DNA or other proteins inside cytoplasm of *E. coli*.

CHAPTER 4

General Conclusion

The results in this thesis revealed the elementary process of bactericidal mechanisms of LfcinB and one of its fragments, LfcinB (4-9). LfcinB induced an influx of membrane impermeant-probe, SYTOX green, to the cytoplasm of the *E. coli* from its surrounding solutions, indicating damage of LfcinB-induced plasma membrane of *E. coli*, whereas LfcinB (4-9) did not induce any damage of the plasma membrane. The results of the interactions of LfcinB and LfcinB (4-9) with GUVs of lipid membrane also support the above data; LfcinB induced local rupture of the membrane of GUVs causing rapid leakage of their internal contents such as calcein and sucrose, whereas LfcinB (4-9) did not induce pore formations in the GUV membrane nor GUV rupture. These result indicate that the key factor of bactericidal activity of LfcinB is the damage of the plasma membrane with its concomittant leakage of internal content of *E. coli*, but that the damage of the plasma membrane is not a source of the bactericidal activity of LfcinB (4-9). On the other hand, I found that Rh-LfcinB (4-9) entered the cytoplasm of *E. coli* and also the lumens of GUVs without leakage of their internal content. These result indicate that Rh-LfcinB (4-9) has a cell-penetrating activity, and hence it can translocate across plasma membrane of *E. coli* and lipid bilayers of GUVs to enter the cytoplasm of *E. coli* and the GUV lumens. Therefore it can be considered reasonably that LfcinB (4-9) can enter the cytoplasm of *E. coli* and bind with DNA or other proteins, which is a key factor for bactericidal activity of LfcinB (4-9). Therefore, it can be concluded that bactericidal mechanisms of LfcinB and LfcinB (4-9) are different irrespective of the same origin.

References:

Adlerova L., Bartoskova A., Faldyna (2008) Lactoferrin: A Review *Veterinarni Medicina 53*, 457-468.

Aguilera, O., Ostolaza, H., Quirós, L. M., and Fierro, J. F. (1999) Permeabilizing action of an antimicrobial lactoferricin-derived peptide on bacterial and artificial membranes, *FEBS Lett. 462*, 273-277.

Ahmad, A., Azmi, S., Srivastava, R. M., Srivastave, S., Pandey, B. K., Saxena, R., Bajpai, V. K., and Ghosh, J. K. (2009) Design of nontoxic analogues of cathelicidin-derived bovine antimicrobial peptide BMAP-27: the role of leucine as well as phenylalanine zipper sequences in determining its toxicity. *Biochemistry 48*, 10905-10917.

Andrews, J. M. (2001) Determination of minimum inhibitory concentrations. *J. Antimicro. Chemo. 48*, S1, 5-16.

Apellániz, B., Nieva, J. L., Schwille, P., and García-Sáez, A. J. (2010) All-or-none versus graded: single-vesicle analysis reveals lipid composition effects on membrane permeabilization, *Biophys. J.*, *99*, 3619-3628.

Bahar, A.A. Ren,D. (2013) Antimicrobial peptides *Pharmaceuticals* 6(12), 1543-1575.

Baker E.N., Baker H.M. (2005): Molecular structure, binding properties and dynamics of lactoferrin. Cellular and Molecular Life Sciences, 62, 2531–2539.

Baker E.N., Baker H.M., (2005) Molecular structure, binding properties and dynamics of lactoferrin. *Cellular and Molecular Life Sciences 62*, 2531–2539.

Baker e.n. (1994): Structure and reactivity of transferrins. Advances in Inorganic Chemistry, 41, 389–463.

Bartlett, G. R. (1959) Phosphorous assay in column chromatography, *J. Biol. Chem. 234*, 466-468.

Bechara, C., and Sagan, S. (2013) Cell-penetrating peptides: 20 years later, where do we stand? *FEBS Lett. 587*, 1693-1702.

Bechinger, B., (2005) Detergent-like properties of magainin antibiotic peptides: A 31p solid-state nmr spectroscopy study. *Biochim. Biophys. Acta,* 1712, 101–108.

Bellamy M., Takase M., Yamauchi K., Wakabayashi H., Kawase K., Tomita M., (1992) Identification of the bactericidal domain of lactoferrin, *Biochim. Biophys. Acta*, *1121*, 130–136.

Bellamy W., Takase M., Wakabayashi H., (1992) Antibacterial spectrum of lactoferricin B, a potent bactericidal peptide derived from the N-terminal region of bovine lactoferrin. *J. Appl Bacteriol 73(6)*, 472–479.

Bennett R. M., Davis J., (1982) Lactoferrin interacts with deoxyribonucleic acid: a preferential reactivity with double-stranded DNA and dissociation of DNA-anti-DNA complexes *J. Lab. Clin. Med. 99 (1)*, 127–138.

Betty R. L., Yue,W. H., Robert, S. A., Han, J. L.(2016) Identification of a Short Cell-Penetrating Peptide from Bovine Lactoferricin for Intracellular Delivery of DNA in Human A549 Cells PLOS ONE | DOI:10.1371/journal.pone.0150439

Boggs, J. M., Euijung, J., Polozov, I. V., Epand, R. F., Anantharamaiah, G. M., Blazyk, J., Epand, R. M. (2001) Effect of magainin, class L, and class A amphipathic peptides on fatty acid spin labels in lipid bilayers. Biochim. Biophys. Acta 1511, 28−41.

Bolintineanu, D.S.; Kaznessis, Y.N. (2011) Computational studies of protegrin antimicrobial peptides: *A review. Peptides 32,* 188–201.

Brock J.H., (1980) Lactoferrin in human milk: its role in iron absorption and protection against enteric infection in the newborn infant. *Archives of Disease in Childhood 55*, 417–421.

Brogden, K.A., (2005) Antimicrobial peptides: Pore formers or metabolic inhibitors in bacteria? *Nat. Rev. Microbiol. 3*, 238–250.

Cevc, G., and Marsh, D. (1987) Phospholipid bilayers, John Wiley and Sons, New York.

Ciobanasu, C., Siebrasse, J. P., and Kubitscheck, U. (2010) Cell-penetrating HIV1 TAT peptides can generate pores in model membranes. *Biophys. J. 99*, 153-162.

Conlon, J.M.; Sonnevend, A., (2010) Antimicrobial peptides in frog skin secretions. *Methods Mol. Biol. 618*, 3–14.

Coscia, A.; Orrù, S.; Di Nicola, P.; Giuliani, F; Rovelli, I; Peila, C; Martano, C; Chiale, F; Bertino, E..J., (2012) Biol Regul Homeost Agents. 26(3 Suppl):39-42.

Domingues, T. M., Riske, K. A., and Milanda, A. (2010) Revealing the lytic mechanism of antimicrobial peptide gomesin by observing giant unilamellar vesicles. *Langmuir 26*, 11077-11084.

Dubey, G. P. and Ben-Yehuda, S. (2011) Intercellular nanotubes mediate bacterial communication. *Cell*, *144*, 590-600.

Ehrenstein, G.; Lecar, H., (1977) Electrically gated ionic channels in lipid bilayers. Q. *Rev. Biophys. 10,* 1–34.

Eliassen, L. T., Berge, G., Leknessuns, A., Wikman, M., Lindin, I., Lekke, C., Ponthan, F., Johnses, J. I., Sveinbjernsson, B., Kogner, P., Flǣgstad, T., and Rekdal, Ǿ. (2006) The antimicrobial peptide, Lfcin B, is cytotoxic to neuroblastoma cells in vitro and inhibits xenograft growth in vivo, *Int. J. Cancer*, *119*, 493-500.

Evans, E., Heinrich, V., Ludwig, F., Rawicz, W. (2003) Dynamic tension spectroscopy and strength of biomembranes. *Biophys. J.*) *85*, 2342-2350.

Evans, E.; Smith, B. A. Kinetics of hole nucleation in biomembrane rupture. *New J. Phys.* (2011) *13*, 095010 (29 pages).

Farge, E., and Devaux, P. F. (1992) Shape changes of giant liposomes induced by an asymmetric transmembrane distribution of phospholipids, *Biophys. J.*, 61, 347-357.

Farnaud, S., Spiller, C., Moriarty, L. C., Patel, A., Gant, V., Odell, E. W., Evans, R. W. (2004) Interactions of lactoferricin-derived peptides with LPS and antimicrobial activity. *FEMS Micro. Lett. 233*, 193-199.

Farrell M., Jamenez-Flores R., Bleck T., Brown M.,Butler E., Creamer K., Hicks L., Hollar M., Ngkwai-Hang F., Swaisgood E., (2004)   Nomenclatue of the proteins of cow's milk-six revision. *J Dairy Sci*. *87,* 1641-1647.

Fuertes, G., Garcia-Sáez, A., Esteban-Martin, S., Giménez, D., Sánchez-Muñoz, O. L., Schwille, P., and Salgado, J. (2010) Pores formed by Baxα5 relax to a smaller size and keep at equilibrium, *Biophys. J.*, *99*, 2917-2925.

Gifford, J. L., Hunter, H. N., and Vogel, H. J. (2005) Lactoferricin: a lactoferrin-derived peptide with antimicrobial, antiviral, antitumor, and immunological properties. *Cell. Mol. Life. Sci. 62*, 2588-2598.

Goins, A. B., Sanabria, H., and Waxham, M. N. (2008) Macromolecular crowding and size effects on probe microviscosity. *Biophys. J.*, *95*, 5362-5373.

Gregory, S. M., Pokorny, A., Almeida, P. F. F. (2009) Magainin 2 revisited: a test of the quantitative model for the   all-or-nonepermeabilization of phospholipid vesicles. Biophys. J. 96, 116−131.

Groves M.L., Peterson R.F., Kiddy C.A., (1965) Poliomorphism in the red protein isolated from milk of individual cows. *Nature, 207,* 1007–1008.

Guyton, A. C. and Hall, J. E. (2006) Textbook of Medical Physiology, 11 ed., Elsevier Saunders, Philadelphia.

He, J., and Furmanski, P. (1995) Sequence specificity and transcriptional activation in the binding of lactoferrin to DNA. *Nature 373*, 721-724.

Heinrich, V., Svetina, S., and Zeks, B. (1993) Nonaxisymmetric vesicle shapes in a generalized bilayer-couple model and the transition between oblate and prolate axisymmetric shapes. *Phys. Rev. E. 48*, 3112-3123.

Hunter, H. N., Demcoe, A. R., Jensen, T. J., Gutteberg, T. J., and Vogel, H. J. (2005) Human lactoferricin is partially folded in aqueous solution and is better stabilized in a membrane mimic solvent, *Antimicrob. Agent Chemothera. 49*, 3387-3395.

Hwang, P. M., Zhou, N., Shan, X., Arrosmith, C. H., and Vogel, H. J. (1998) Three-dimensional solution structure of lactoferricin B, an antimicrobial peptide derived from bovine lactoferrin, *Biochemistry 37*, 4288-4298.

Hwang, P. M., and Vogel, H. J. (1998) Structure-function relationships of antimicrobial peptides, *Biochem. Cell Biol.* 76, 235-246.

Islam, M. Z., Alam, J. M., Tamba, Y., Karal, M. A. S., Yamazaki, M. (2014) The single GUV method for revealing the functions of antimicrobial, pore-forming toxin, and cell-penetrating peptides or proteins. *Phys. Chem. Chem. Phys.*, 16, 15752-15767.

Islam, M. Z., Alam, J. M., Tamba, Y., Karal, M. A. S., and Yamazaki, M.(2014,) The single GUV method for   revealing the functions of antimicrobial, pore-forming toxin, and cell-penetrating peptides or proteins. *Phys. Chem. Chem. Phys.*, *16*, 15752-15767.

Islam, M. Z., Ariyama, H., Alam, J. M., and Yamazaki, M. (2014) Entry of cell-penetrating peptide transportan 10 into a single vesicle by translocating across lipid membrane and its induced pores. *Biochemistry*, *53*, 386-396.

Israelachvili J.N., (1992) Intermolecular and surface forces, 2nd Ed., Academic Press, New York.

Jenson H., Hamil P., and Hancock R.E.W., (2006) Peptide antimicrobial agents. *Clinical microbiology reviews 19(3),* 491-511.

Jing, W., Svendsen, J. S., and Vogel, H, J. (2006) Comparison of NMR structures and model-membrane interactions of 15-residue antimicrobial peptides derived from bovine lactoferricin, *Biochem. Cell Biol*. *84*, 312-326.

Kang, J. H., Lee, M. K., Kim, K. L., and Hahm, K. –S. (1996) Structure-biological activity relationships of 11-residue highly basic peptide segment of bovine lactoferrin, *Int. J. Pept. Protein Res.*, *48*, 357-363.

Kanyshkova, T. G., Semenov, D. V., Buneva, V. N., and Nevinsky, G. A. (1999) Human milk lactoferrin binds two DNA molecules with different affinities. *FEBS Lett. 451*, 129-141.

Karal, M. A. S., Levadny, V., Tsuboi, T., Belays, M., and Yamazaki, M. (2015) Electrostatic interaction effects on tension-induced pore formation in lipid membranes, *Phys. Rev. E.*, 92, 012708 (7 pages).

Karal, M. A. S., Alam, J. M., Takahashi, T., Levadny, V., and Yamazaki, M. (2015) Stretch-Activated Pore of Antimicrobial Peptide Magainin 2, *Langmuir*, *31*, 3391-3401.

Karal, M. A. S., Levadnyy, V., and Yamazaki, (2016) M. Analysis of Constant Tension-Induced Rupture of Lipid Membranes Using Activation Energy. *Phys. Chem. Chem. Phys*. *18*, 13487-13495.

Karatekin, E., Sandre, O., Guitouni, H., Borghi, N., Puech, P. –H., Brochard-Wyard, F. Cascades of transient pores in giant vesicles: line tension and transport. *Biophys. J.* (2003) *84*, 1734-1749.

Kikuchi M., Mizoroki S., Kubo T., Ohiwa Y., Kubota M., Yamada N., Orino K., Ohnami Y., Watanabe K. (2003): Seminal plasma lactoferrin but not transferrin reflects gonadal function in dogs. The Journal of Veterinary Medical Science, 65, 679–684.

Koren, E., and Torchilin, V. P. (2012) Cell-penetrating peptides: breaking through to the other side. *Trends. Mol. Med*. 18, 385-393.

Kuwata, H., Yip, T. T., Tomita, M., and Hutchens, T. W. (1998) Direct evidence of the generation in human stomach of an antimicrobial peptide domain (lactoferricin) from ingested lactoferrin, *Biochim. Biophys. Acta*, *1429*, 129-141.

Leippe, M., (1999) Antimicrobial and cytolytic polypeptides of amoeboid protozoa— Effector molecules of primitive phagocytes. *Dev. Comp. Immunol. 23,* 267–279.

Levadny, V., Tsuboi, T., Belaya, M., Yamazaki, M. Rate constant of tension-induced pore formation in lipid membranes, *Langmuir* (2013) *29*, 3848-3852.

Levay p.f., viljoen m. (1995): Lactoferrin: a general review. Haematologica, 80, 252–267. Lonnerdal B., Iyer S. (1995): Lactoferrin: molecular structure and biological function. Annual Review of Nutrition, 15, 93–110.

Lister, J. D. Stability of lipid bilayers and red blood cell membranes, *Phys. Lett.* (1975) *A53*, 193- 194.

Liu, B. R.; Huang, Y.-W., Aronstam, R. S., and Lee. H. –J. (2016) Identification of a short cell-penetrating peptide from Bovine lactoferricin for intracellular delivery of DNA in human A 549 cells, *Plos one*, *11*, e0150439.

Lonnerdal B., Iyer S. (1995): Lactoferrin: molecular structure and biological function. Annual Review of Nutrition, 15, 93–110.

Lopez-Montero, I., Rodriguez, N., Cribier, S., Pobl, A., Velez, M., and Devaux, P. F. (2005) Rapid transbilayer movement of ceramides in phospholipid vesicles an d in human erythrocytes, *J. Biol. Chem.*, 280, 25811-25819.

Lopez-Montero, I., Rodriguez, N., Cribier, S., Pobl, A., Velez, M., and Devaux, P. F. (2005) Rapid transbilayer movement of ceramides in phospholipid vesicles and in human erythrocytes, *J. Biol. Chem.*, 280, 25811-25819.

Magzoub, M., and Gräslund, A. (2004) Cell-penetrating peptides: small from inception to application. *Quart. Rev. Biophys.* 37, 147-195.

Masson P.L., Heremans J.F. (1971) Lactoferrin in milk from different species. Comparative Biochemistry and Physiology. B, *Comparative Biochemistry*, *39,* 119–129.

Masson P.L., Heremans J.F., Dive C. (1966) An ironbinding protein common too many external secretions. *Clinica Chimica Acta, 14,* 735–739.

Masson P.L., Heremans J.F., Dive C. (1966): An ironbinding protein common to many external secretions. Clinica Chimica Acta, 14, 735–739.

Masson, P. L., Heremans, J. F., and Dive, C. H. (1966) An iron-binding protein common to many external secretions, *Clin. Chim. Acta 13*, 735-739.

Masson, P. L.; Heremans, J. F.; Dive, C. H. An iron-binding protein common to many external secretions, *Clin. Chim. Acta* **1966**, *13*, 735-739.

Masum, S. M., Li, S. J., Tamba, Y., Yamashita, Y., Tanaka, T., and Yamazaki, M. (2003) Effect of de Novo Designed Peptides Interacting with the Lipid-Membrane Interface on the Stability of the Cubic Phases of the Monoolein Membrane, *Langmuir*, 19, 4745-4753.

Matsuzaki, K., Murase, K., Fujii, N., Miyajima, K. (1995) Translocation of a channel-forming antimicrobial peptide, magainin 2, across lipid bilayers by forming a pore. Biochemistry 34, 6521−6526.

Matsuzaki, K., Sugishita, K., Ishibe, N., Ueha, M., Nakata, S., Miyajima, K., Epand, R. M. (1998) Relationship of membrane curvature to the formation of pores by magainin 2. Biochemistry 37, 11856−11863.

Matsuzaki, K.; Murase, K.; Fujii, N.; Miyajima, K. Translocation of a channel-forming antimicrobial peptide, magainin 2, across lipid bilayers by forming a pore. *Biochemistry* **1995**, *34*, 6521-6526.

McLaughlin, S., and Murray, D. (2005) Plasma membrane phosphoinositide organization by protein electrostatics, *Nature*, 438, 605-611.

Mecke, A.; Lee, D.K.; Ramamoorthy, A.; Orr, B.G.; Holl, M.M.B., (2005) Membrane thinning due to antimicrobial peptide binding: An atomic force microscopy study of msi-78 in lipid bilayers. *Biophys. J. 89,* 4043–4050.

Melo, M. N., Ferre, R., and Castanho, A. R. B. (2009) Antimicrobial peptides: linking partition, activity and high membrane-bound concentrations, *Nat. Rev. Microbiol. 8*, 1-5.

Metz-Boutique M.H., Jolles J., Mazurier J., Schoentgen F., Legrand D., Spik G., Montreuil J., Jolles P. (1984) Human lactotransferrin: amino acid sequence and structural comparisons with other transferrins. *European Journal of Biochemistry, 145*, 659–676.

Miao, L., U. Seifert, M. Wortis, and H.-G. Döbereiner. (1994) Budding transitions of fluid-bilayer vesicles: The effect of area-difference elasticity. *Phys. Rev. E. 49*, 5389-5407.

Mishra, A., Gordon, V. D., Yang, L., Coridan, R., and Wong, G. C. L. (2008) HIV TAT forms pores in membranes by inducing saddle-spray curvature: potential role of bidentate hydrogen bonding. *Angew. Chem. Int. Ed., 47*, 2986-2989.

Mishra, A., Lai, G. H., Schmidt, N. W., Sun, V. Z., Rodriguez, A. R., Tong, R.;, Tang, L., Cheng, J., Deming, T. J., Kamei, D. T., and Wong, G. C. L. (2011) Translocation of HIV TAT peptide and analogues induced by multiplexed membrane and cytoskeletal interactions, *Proc. Natl. Acad. Sci. USA*, *108*, 16883-16888.

Moniruzzaman, M.; Alam, JK. M.: Dohra, H.; Yamazaki, M. Antimicrobial peptide lactoferricin B-induced rapid leakage of internal contents from single giant unilamellar vesicles. *Biochemistry*, **2015**, *54*, 5802-5814.

Mukherjee, S., Zheng, H., Derebe, M. G., Callenberg, K. M., Patch, C. L., Rollins, D., Propheter, D., Rizo, J., Grabe, M., Jiang, Q.-X., and Hooper, L. V. (2014) Antibacterial membrane attack by a pore-forming intestinal C-type lectin, *Nature 305*, 103-107.

Nguyen L., Chau J., Perry N., (2010) Serum stabilities of short tryptophan-and arginine-rich antimicrobial peptide analoge. *Plos One 5(9)* 12684.

Nguyen, L. T., Schibli, D., and Vogel, H. J. (2005) Structural studies and model membrane interactions of two peptides derived from lactoferricin, *J. Peptide Sci.*, *11*, 379-389.

Oka, T., Tsuboi, T., Saiki, T., Takahashi, T., Alam, J. M., and Yamazaki, M. (2014) Initial Step of pH-Jump-Induced Lamellar to Bicontinuous Cubic Phase Transition in Dioleoylphosphatidylserine/ Monoolein. *Langmuir 30*, 8131-8140.

Orsi N., (2004) The antimicrobial activity of lactoferrin: current status and perspectives Biometals 17(3), 189-196.

Pammi M, Abrams S., (2009) Oral lactoferrin for the treatment of sepsis and necrotizing enterocolitis in neonates. *Cochrane Database Syst Rev 1;* 138.

Park, C. B.; Yi, K.-S.; Matsuzaki, K.; Kim, M. S.; Kim, S. C., (2000) Structure-activity analysis of buforin II, a histone H2A-derived antimicrobial peptide: The proline hinge is responsible for the cell-penetrating ability of buforin II. *Proc. Natl. Acad. Sci. USA. 97*, 8245-8250.

Peters, B.M., Shirtliff, M.E., Jabra-Rizk, M.A., (2010) Antimicrobial peptides: Primeval molecules or future drugs? PLoS Pathogens. 6(10), e1001067 (1-4).

Pisa, M. D., Chassaing, G., and Swiecicki, J.-M. (2015) Translocation mechanism(s) of cell-penetrating peptides: biophysical studies using artificial membrane bilayers. *Biochemistry*, 54, 194-207.

Pouny, Y., Rapaport, D., Mor, A., Nicolas, P., and Shai, Y. (1992) Interaction of antimicrobial dermaseptin and its fluorescently labeled analogues with phospholipid membranes. *Biochemistry 51*, 12416-12423.

Pushpanathan, M., Rajendhran, J., Jayashree, S., Sundarakrishnan, B., Jayachandran, S., Gunasekaran, P., (2012) Identification of a novel antifungal peptide with chitin-binding property from marine metagenome. *Protein Pept. Lett. 19,* 1289–1296.

Radek, K.,Gallo, R., (2007) Antimicrobial peptides: Natural effectors of the innate immune system. *Semin. Immunopathol. 29,* 27–43.

Rekdal, Ǿ., Andersen, J., Vorland, L. H., and Svendsen, J. S. (1999) Construction and synthesis of lactoferricin derivatives with enhanced antibacterial activity, *J. Pept. Sci. 5*, 32-45.

Rosenmund A, Kuyas C, Haeberli A (1986) Oxidative radioiodination damage to human lactoferrin. *Biochem. J. 240 (1)* 239–45.

Roth, B. L., Poot, M., Yue, S. T., and Millard, P. J. (1997) Bacterial viability and antibiotic susceptibility testing with SYTOX green nucleic acid stain. *App. Env. Microbiol. 63*, 2421-2431.

Saito A, Ueda K, Imamura M (2004) Purification and cDNA cloning of a novel antibacterial peptide with a cysteine-stabilized alphabeta motif from the longicom beetle, Acalolepta luxuriosa. *Dev Comp Immunol 28*, 1–7.

Sandre, O., Moreaux, L., Brochard-Wyard, F. Dynamics of transient pores in stretched vesicles. *Proc. Natl. Acad. Sci. USA*. (1999) *96*, 10591-10596.

Schauber, J.; Gallo, R.L. *(*2008) Antimicrobial peptides and the skin immune defense system. J. Allergy Clin. Immunol 122*, 261–266.

Schibili D. J., Hwang P.M., Vogel H.J., (1999) The structure of antimicrobial active center of Lactoferricin B bound to sodium dodecyl sulfate micelles *FEBS Lett 446(2-3)*, 213-217.

Schibli, D. J., Epand, R. F., Vogel, H. J., and Epand, R. M. (2002) Tryptophan-rich antimicrobial peptides: comparative properties and membrane interactions. *Biochem. Cell. Biol. 80*, 667-677.

Schön, A. J. Garcia-Saez, P. Malovrh, K. Bacia, G. Anderluh, and P. Schwille, (2008) Equinatoxin II Permeabilizing activity depends on the presence of sphingomyelin and lipid phase coexistence, *Biophys. J.*, *95*, 691-698.

Shai Y., (1999) Mechanism of the binding, insertion and destabilization of phospholipid bilayer membranes by K-helical antimicrobial and cell non-selective membrane-lytic peptides *Biochimica et Biophysica Acta* 1462 55-70.

Sharmin, S.; Islam, M. Z.; Karal, M. A. S.; Shibly, S. U. A.; Dohra, H.; Yamazaki, M. Effects of lipid composition on the entry of cell-penetrating peptide oligoarginine into single vesicles. *Biochemistry*, **2016**, 55, 4154-4165.

Shimazaki, K.; Tazume, T.; Uji, K.; Tanaka, M.; Kumura, H.; Mikawa, K.; Shimo-Oka, T., (1998) Properties of a heparin-binding peptide derived from bovine lactoferrin. *J. Dairy. Sci. 81,* 2841–2849.

Sochacki, K. A.; Barns, K. J.; Bucki, R.; Weisshaar, J. C. Real-time attack on single Escherichia coli cells by the human antimicrobial peptide LL-37. *Proc. Natl. Acad. Sci. USA.* **2011**, *108*, E77-E81.

Stanzl, E. G., Trantow, B. M., Vargas, J. R., and Wender P. A. (2013) Fifteen years of cell-penetrating, guanidinium-rich molecular transporters: basic science, research tools, and clinical applications. *Acc. Chem. Res.* 46, 2944-2954.

Strǿm, M. B., Haug, B. E., Rekdal, Ǿ., Skar, M. L., Strensen, W., and Svendsen, J. S. (2002) Important structural features of 15-residue lactoferricin derivatives and methods for improvement of antimicrobial activity, *Biochem. Cell Biol. 80*, 65-74.

Strǿm, M. B., Rekdal, Ǿ., and Svendsen, J. S. (2000) Antibacterial activity of 15-residue lactoferricin derivatives, *J. Pept. Res. 56*, 265-274.

Tamba, Y., Ariyama, H., Levadny, V., and Yamazaki, M. (2010) Kinetic pathway of antimicrobial peptide magainin 2-induced pore formation in lipid membranes. *J. Phys. Chem. B*. 114, 12018-1202

Tamba, Y., Ohba, S., Kubota, M., Yoshioka, H., Yoshioka, H., and Yamazaki, M. (2007) Single GUV method reveals interaction of Tea catechin (-)-epigallocatechin gallate with lipid membranes. *Biophys. J. 92*, 3178-3194.

Tamba, Y., Terashima, H., and Yamazaki, M. (2011) A membrane filtering method for the purification of giant unilamellar vesicles. *Chem. Phys. Lipids 164*, 351-358.

Tamba, Y., and Yamazaki, M. (2005) Single giant unilamellar vesicle method reveals effect of antimicrobial peptide, magainin-2, on membrane permeability. *Biochemistry 44*, 15823- 15833.

Tamba, Y., and Yamazaki, M. (2009) Magainin 2-induce pore formation in the lipid membranes depends of its concentration in the membrane interface. *J. Phys. Chem. B 113*, 4846-4852.

Tanaka, T., Sano, R., Yamashita, Y., and Yamazaki, M. (2004) Shape changes and vesicle fission of giant unilamellar vesicles of liquid-ordered phase membrane induced by lysophosphatidylcholine. *Langmuir 20*, 9526-9534.

Tanaka, T., Tamba, Y., Masum, S. M., Yamashita, Y., and Yamazaki, M. (2002) La^{3+} and Gd^{3+} induce shape change of giant unilamellar vesicles of phosphatidylcholine. *Biochim. Biophys. Acta 1564*, 173-182.

Taupin, C., Dvolaitzky, M., Sauterey, C., (1975) Osmotic pressure induced pores in phospholipid vesicles, *Biochemistry14*, 4771-4775.

Tomita M., Takase M., Bellamy W., (1994) A review: The active peptide of lactoferrin. Acta Paediatr Jpn 36(5), 585-591.

Tomita, M .W. Bellamy, M. Takase, K. Yamauchi, H. Wakabayashi, K., (1991) Potent antibacterial peptides generated by pepsin digestion of bovine lactoferrin *J. Dairy Sci., 74,* 4137–4142

Tomita, M., Takase, M., Bellamy, W., and Shimamura, S. (1994) A review: The active peptide of lactoferrin, *Acta Paediatr. J. 36*, 585-591.

Tomita, M., Wakabayashi, H., Shin, K., Yamauchi, K., Yaeshima, T., and Iwatsuki, K. (2009) Twenty-five years of research on bovine lactoferrin applications. *Biochimie*, *91*, 52-57.

Ueta E., Tanida T., Osaki T., (2001) A novel bovine lactoferrin peptide, FRCRRWQWRM, suppresses Candida cell growth and activates neutrophils. *J Peptides Res 57(3),* 240-249.

Ulvatne H, Haukland HH, Olsvik Ø, Vorland LH (2001) Lactoferricin B causes depolarization of the cytoplasmic membrane of *Escherichia coli* ATCC 25922 and fusion of negatively charged liposomes. *FEBS Lett 492(1–2):*62–65.

Umeyama, M., Kira, A., Nishimura, K., and Naito, A. (2006) Interactions of bovine lactoferricin with acidic phospholipid bilayers and its antimicrobial activity as studied by solid-state NMR, *Biochim. Biophys. Acta 1758*, 1523-1528.

Vogel, H. J., Schibli, D. J., Jing, W., Lohmeirer-Vogel, E. M. Epand, R. F., and Epand, R. M. (2002) Towards a structure-function analysis of bovine lactoferricin and related tryptophan- and arginine-containing peptides. *Biochem. Cell. Biol. 80*, 49-63.

Wade, D.; Boman, A.; Wahlin, B.; Drain, C. M.; Andreu, A.; Boman, H. G.; Merrifield, R. B. All-D amino acid-containing channel-forming antibiotic peptides. *Proc. Natl. Acad. Sci. USA.* **1990**, *87*, 4761-4765.

Wakabayashi, H M. Takase, M. Tomita (2003) Lactoferricin derived from milk protein lactoferrin *Curr. Pharm. Des., 9*, 1277–1287.

Wakabayashi, H., Matsumoto, H., Hashimoto, K., Teraguchi, S., Takase, M., and Hayasawa, H. (1999) N-acylated and D enantiomer derivatives of a nonamer core peptide of lactoferricin B showing improved antimicrobial activity, *Antimicrob. Agents Chemothera. 43*, 1267-1269.

Wakabayashi, H., Takase, M., and Tomita, M. (2003) Lactoferricin derived from milk protein lactoferrin, *Curr. Pharm. Des. 9*, 1277-1287.

Ward, P.P.; Paz, E.; Conneely, O.M., (2005) *Cell. Mol. Life Sci* 62: 2540.

Wimley, W. C., and White, S. H. (1996) Experimentally determined hydrophobicity scale for proteins at membrane interface, *Nature Struct. Biol. 3*, 842-848.

Wu, M.; Maier, E.; Benz, R.; Hancock, R.E. (1999) Mechanism of interaction of different classes of cationic antimicrobial peptides with planar bilayers and with the cytoplasmic membrane of *Escherichia coli. Biochemistry 38,* 7235–7242.

Yamashita, Y., Masum, S. M., Tanaka, T., and Yamazaki, M. (2002) Shape changes of giant unilamellar vesicles of phosphatidylcholine induced by a de novo designed peptide interacting with their membrane interface, *Langmuir 18*, 9638-9641.

Yamauchi, K., Tomita, M., Giehl, T. J., and Ellison III, R. T. (1993) Antibacterial activity of lactoferrin and a pepsin-derived lactoferrin peptide fragment. *Inf. Immu. 61*, 719-728.

Yamazaki, M. (2008) The single GUV method to reveal elementary processes of leakage of internal contents from liposomes induced by antimicrobial substances, *Adv. Planar Lipid Bilayers and Liposomes*, *7*, 121-142.

Yamazaki, M., and Ito, T. (1990) Deformation and instability in membrane structure of phospholipid vesicles caused by osmophobic association: Mechanical stress model for the mechanism of poly (ethylene glycol)-induced membrane fusion, *Biochemistry*, 29, 1309-1314.

Yu K., Kim K., Lee J., (2002) Comparative study on characteristics of lysozymes from the hemolymph of three lepidopteran larvae, Galleria mellonella, Bombyx mori, Agrius convolvuli. *Dev Comp Immunol 26*,707–713.

Zasloff, M. (2002) Antimicrobial peptides of multicellular organisms. *Nature 415*, 389-395.

Zhang, L.; Rozek, A.; Hancock, R.E., (2001) Interaction of cationic antimicrobial peptides with model membranes. *J. Biol. Chem. 276,* 35714–35722.

Zhao, X.; Wu, H.; Lu, H.; Li, G.; Huang, Q. Lamp (2013) A database linking antimicrobial peptides. PLoS One8, e66557.

Zorko, M., and Langel, Ű. (2005) Cell-penetrating peptides: mechanism and kinetics of cargo delivery. *Adv. Drug. Deliv. Rev.* 57, 529-545.

Acknowledgement

It gives me immense pleasure in expressing my gratitude to all those people who have supported me and had their contributions in making this thesis possible.

Firstly, I would like to express my deep and sincere gratitude to my supervisor, Professor Dr. Masahito Yamazaki, Department of Bioscience, Graduate School of Science & Technology, Shizuoka University, for his wise supervision, important suggestions and proper guidance throughout the study.

Secondly, I would like to acknowledge Dr. Hideo Dohra for his cooperation during entire period of the research work. I would also like to express my special thanks to Dr. Jahangir Alam and Dr. Zahidul Islam for their cooperation.
My warm thanks to all of my lab members for their valuable suggestions and friendly help.

Finally, I must acknowledge and thank the Almighty Allah for blessing, protecting and guiding me throughout the period of my doctoral research work.

Md. Moniruzzaman